

Wet granular materials

NAMIKO MITARAI*† and FRANCO NORI‡§

†Department of Physics, Kyushu University 33, Fukuoka 812-8581, Japan
‡Frontier Research System, The Institute of Physical and Chemical Research
(RIKEN), Hirosawa 2-1, Wako-shi, Saitama 351-0198, Japan
§Center for Theoretical Physics, Physics Department, Center for the Study
of Complex Systems, The University of Michigan, Ann Arbor,
Michigan 48109-1040, USA

(Received 26 July 2005; in final form 2 September 2005)

Most studies on granular physics have focused on dry granular media, with no liquids between the grains. However, in geology and many real world applications (e.g. food processing, pharmaceuticals, ceramics, civil engineering, construction, and many industrial applications), liquid is present between the grains. This produces inter-grain cohesion and drastically modifies the mechanical properties of the granular media (e.g. the surface angle can be larger than 90 degrees). Here we present a review of the mechanical properties of wet granular media, with particular emphasis on the effect of cohesion. We also list several open problems that might motivate future studies in this exciting but mostly unexplored field.

Keywords: Granular material; Wet grains; Cohesion

	Contents	PAGE
1.	Introduction	2
1.1.	Granular physics and wet granular media	2
1.2.	What is different from dry granular media?	3
2.	Wet granular media: Grains with liquid and air	5
2.1.	Cohesion between two spheres	5
2.1.1.	Meniscus and suction	5
2.1.2.	Liquid bridge between two spheres	6
2.2.	Wet granular media with various liquid content	7
2.2.1.	Four states of liquid content: pendular, funicular, capillary, and slurry state	7
2.2.2.	Liquid content and suction	8
2.2.2.1.	Measurement of suction in granular media	8
2.2.2.2.	Relation between the liquid content and suction	10
3.	Mechanical properties	12
3.1.	Granular cohesion in the static and quasi-static regimes	12
3.1.1.	Compaction of wet granular media	12
3.1.2.	Angle of repose for small amounts of liquid	13

*Corresponding author. Email: namiko@stat.phys.kyushu-u.ac.jp

3.1.2.1. Experiments	13
3.1.2.2. Cohesion and angle of repose	14
3.1.3. Tensile, compression, and shear tests for intermediate and large liquid content	19
3.1.3.1. Test methods and Mohr circle	19
3.1.3.2. Tests in the pendular state	23
3.1.3.3. Tests with intermediate liquid content	24
3.1.3.4. Tests in soil mechanics: relatively large amounts of liquid	25
3.2. Dynamical behaviour	27
3.2.1. Dynamics in the pendular state	28
3.2.1.1. Avalanches in rotating drums	28
3.2.1.2. Vibrated wet granular media	29
3.2.1.3. Segregation	31
3.2.2. Shear experiments for various liquid content	32
3.2.3. Dynamics of wet granular media: practical applications	35
3.2.3.1. Agglomeration processing: grains bound by liquid	35
3.2.3.2. Geological events	35
4. Summary and open questions	35
4.1. Effect of the liquid content on quasi-static behaviour	35
4.2. Open problems	36
4.2.1. Jamming	37
4.2.2. Statistical mechanics approach	39
4.2.3. Arches and contact-force fluctuations	39
4.2.4. Simple experimental set-ups to study the dynamics of wet granular media	39
4.2.5. Numerical simulations	40
4.2.6. Mechanical properties of snow	40
5. Conclusion	41
Acknowledgements	41
References	41

1. Introduction

1.1. Granular physics and wet granular media

Granular materials are collections of macroscopic particles, like glass beads or sand, which are visible to the naked eye. Because of the macroscopic size of the particles, thermal noise plays no role in particle motion, and particle–particle interactions are dissipative. Therefore, continuous energy input by external forces (gravity, vibrations, etc.) are necessary in order to keep them in motion. Particles may stay at rest like a solid, flow like a liquid, or behave like a gas, depending on the rate of energy input. However, the external force is often not enough for the particles to explore their phase space, which makes them quite different from conventional molecular systems.

The scientific study of granular media has a long history, mainly in the engineering field, and many physicists have joined the granular research community over the past few decades (for reviews and books, see, e.g. [1–12]). Most studies on granular media, especially in the physics field, have focused on *dry granular materials*, where the effects of interstitial fluids are negligible for the particle dynamics. For dry granular media, the dominant interactions are inelastic collisions

and friction, which are short-range and *non-cohesive*. Even in this idealized situation, dry granular media show unique and striking behaviour, which have attracted the attention of many scientists for centuries.

In the real world, however, we often see *wet granular materials*, such as beach sand. Dry and wet granular materials have many aspects in common, but there is one big difference: Wet granular materials are *cohesive* due to surface tension.

In the past, many research groups that studied granular physics have been struggling to minimize humidity and avoid inter-granular cohesive forces (e.g. [13]). Indeed, some experiments were performed in vacuum chambers. Humidity and fluids in general were seen as a nuisance to be avoided at all costs. However, many important real life applications involve mechanical properties of wet granular media. Examples include rain-induced landslides, pharmaceuticals, food processing, mining and construction industries. Thus, it is important to study the mechanical response of granular matter with various degrees of wetness or liquid content.

In this review, we show how the cohesion induced by the liquid changes the mechanical properties of granular materials. We mainly consider static or quasi-static situations, where the cohesion dominates over other effects of the liquid, such as lubrication and viscosity. Some phenomena in this field which are not well-understood are presented below as ‘open problems’. Most references listed at the end focus on experimental results. Theoretical approaches can be found in the reviews cited below and references therein.

1.2. What is different from dry granular media?

Studies of wet granular media have been made in many industrial applications. The mechanical properties of wet granular media are also extremely important in geology and civil engineering. For example, let us consider a huge and expensive civil works project, the construction of the Kansai International Airport, on a man-made island near Osaka. The weight of the 180 million cubic metres of landfill and facilities compressed the seabed, composed of clay, inevitably causing the airport to sink by some amount. The airport had sunk by 11.7 metres on average at the end of 2000, and the settlement is still carefully monitored [14]. This with other examples from geology and civil engineering stress the need to better understand the mechanical properties of wet granular assemblies, both small and large.

The biggest effect that the liquid in granular media induces is the cohesion between grains. Even humidity in the air may result in a tiny liquid bridge at a contact point, which introduces cohesion. The cohesion occurs in wet granular material unless the system becomes overwet, i.e. the granular medium is completely immersed in a liquid. In this short review, we focus on the effect of this cohesion; the system that we are considering is partially wet granular material, which is a mixture of solid grains, liquid, and air.

In addition to cohesion, there are many effects induced by the presence of the liquid. One of them is the lubrication of solid–solid friction [15–17]. In addition, the liquid viscosity may induce velocity-dependent behaviour and additional dissipation. These effects are often seen in underwater experiments (e.g. [18, 19]). The time-scale of liquid motion (how the liquid moves or flows through granular media) also affects the dynamics. All of these effects, of course, play important

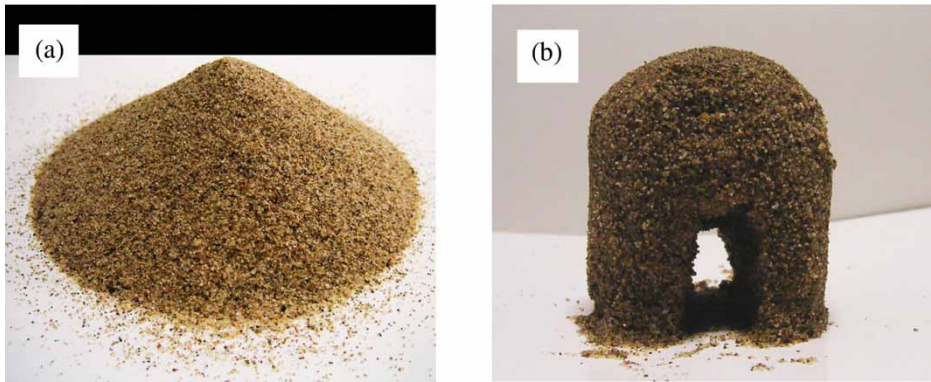


Figure 1. (colour online). (a) Dry sandpile with a well-defined surface angle. (b) Wet sandpile with a tunnel.

roles in the properties of wet granular media. However, these are more or less velocity-dependent phenomena; in the static or quasi-static regime, the cohesion often plays the most important role, providing a significant qualitative difference from dry granular media.

The simplest situation where we see the effect of cohesion in wet granular media would be the sandpiles that children make in a sandbox. Let us first consider a sandpile made of dry grains, and afterwards wet grains.

When we make a sandpile using dry sand (figure 1(a)), the surface of the pile is smooth, making a finite, well-defined angle, which is about 35° . A slightly denser pile might be made by tapping the surface, but would not change the shape of the pile by much. Even if we try to make a sharper pile by pouring more dry sand, grains flow down along the pile surface, and the resulting angle is always around the same value. It is easy to remove part of the sand from the pile, but we cannot make a tunnel through a dry sandpile because the wall around the hole would collapse, and the angle of the surface cannot be larger than the critical angle.

Let us add some water to the sand, and make another sandpile (figure 1(b)). We can try to find the optimal amount of water to produce a certain shape. Small amounts of water do not allow the creation of many shapes, while too much water results in muddy water that cannot keep a shape. With the proper amount of water, we can make a sandpile with the surface angle larger than the dry case. Indeed, the angle can be as large as 90° , or even larger, allowing the construction of elaborate and stunning sandcastles (see, e.g. figure 2). This wet pile can be made denser and stronger by tapping the surface. Now we can make a tunnel through the pile, if we are sufficiently careful. If we try to make a hole that is too large, the pile would break down, forming some rugged surfaces.

Therefore, in a sandbox, we already learnt important properties of dry granular media: a finite angle of repose, small hysteresis in packing, and small strength against loading. We also learnt how drastically these properties are changed or enhanced by adding a liquid, resulting in: a much larger angle of repose, stronger hysteresis in packing, and enhanced strength against loading. These comparisons are summarized in table 1. In the following sections, we will see how this behaviour is studied by scientists.

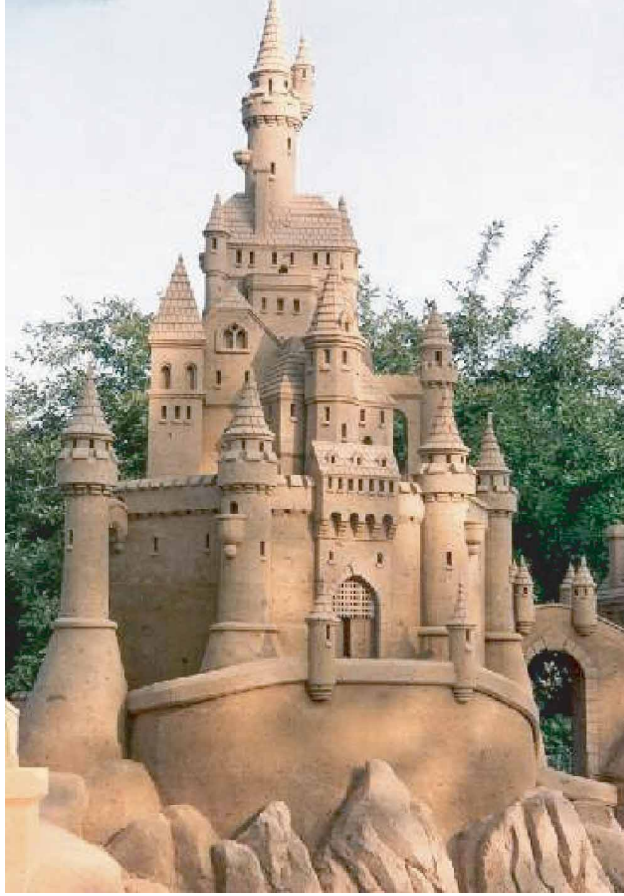


Figure 2. Sandcastle made of wet sand (Copyright Sandscapes 2005).

2. Wet granular media: Grains with liquid and air

2.1. Cohesion between two spheres

2.1.1. Meniscus and suction. Cohesion in wet granular media arises from surface tension and capillary effects of the liquid. Consider a meniscus between air with pressure P_a and liquid with pressure P_l . The pressure difference ΔP between liquid and air with a meniscus of curvature radii r_1 and r_2 is given by the Young–Laplace equation as

$$\Delta P = P_a - P_l = \gamma \left[\frac{1}{r_1} + \frac{1}{r_2} \right], \quad (1)$$

where γ is the surface tension between air and the liquid, and the curvature is positive when the meniscus is drawn back into the liquid phase (e.g. [20]). When the curvature is positive, ΔP is positive, and it is often called the suction.

Table 1. Comparison of physical properties between dry and wet granular matter.

Property	Dry	Wet
Cohesion	Negligible	Important
Surface angle	Finite around 35° for sand	Finite: Larger than the dry case Can be as large as 90°, or even larger
Tensile strength	Negligible	Finite
Yield shear stress	Finite Zero at zero normal stress	Finite: Can be larger than the dry case Non-zero at zero normal stress
Hysteresis	Yes	Yes: Enhanced
Configurational phase space for packing	Finite	Finite: Can be larger than the dry case

The capillary length

$$a = \sqrt{\frac{2\gamma}{\rho_l g}} \quad (2)$$

gives the length-scale that compares the capillary force and gravity, where g is the gravitational acceleration and ρ_l is the mass density of the liquid; a is around 3.9 mm for water at room temperature. The capillary force becomes dominant when the relevant length scales are much smaller than a . Hereafter we consider the situation where the capillary force is dominant. In general, one needs to consider the capillary length when interpreting experimental results, because most experiments are conducted under gravity.

2.1.2. Liquid bridge between two spheres. Now let us see how the liquid induces cohesion in granular media by considering a liquid bridge between two identical spheres as shown in figure 3. The attracting force between spheres due to the liquid menisci is given by the sum of the surface tension and the suction; when we estimate the force at the neck of the bridge, it is given by

$$F_{\text{bridge}} = 2\pi r_2 \gamma + \pi r_2^2 \Delta P, \quad (3)$$

with

$$\Delta P = \gamma \left[\frac{1}{r_1} - \frac{1}{r_2} \right]. \quad (4)$$

The detailed experimental analysis of the cohesion force due to the liquid bridge between two spheres is found in [21]. The effect of roughness on the cohesive force is discussed in detail in [22].

In real partially wet granular media, the picture of a liquid bridge formed between completely spherical particles is often not sufficient to describe the interaction. However, the presence of a liquid, which tries to minimize its surface area, generally results in suction and a cohesive force between particles.

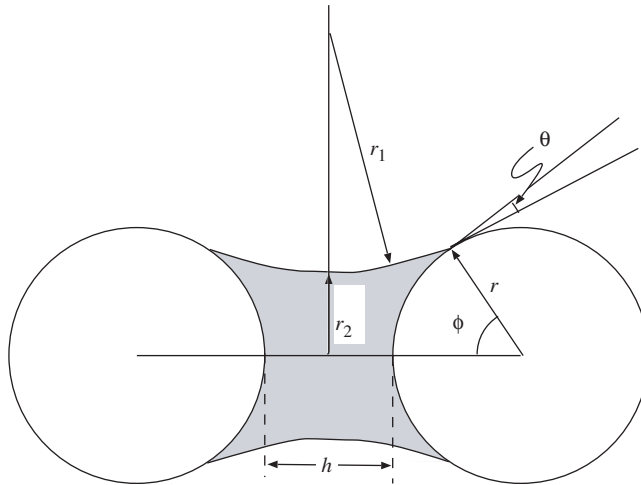


Figure 3. Schematic diagram of a liquid bridge between identical spheres.

2.2. Wet granular media with various liquid content

2.2.1. Four states of liquid content: pendular, funicular, capillary, and slurry state. It is well known that cohesion in wet granular materials depends on the amount of liquid in the system. The following four regimes of liquid content have been distinguished in wet granular media [23, 24]:





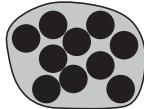
- Pendular state: Particles are held together by liquid bridges at their contact points.
- Funicular state: Some pores are fully saturated by liquid, but there still remain voids filled with air.
- Capillary state: All voids between particles are filled with liquid, but the surface liquid is drawn back into the pores under capillary action.
- Slurry state: Particles are fully immersed in liquid and the surface of liquid is convex, i.e. no capillary action at the surface.

These four regimes are schematically shown in table 2.

Cohesion arises in the pendular, funicular, and capillary states. Thus, we consider these three states in this review. *A priori*, the mechanical properties of these three states would be expected to be qualitatively different. In the case of the pendular state, the cohesive force between a pair of grains acts through a liquid bridge; while in the capillary state the interface between the liquid and the air is pressed due to the suction, and that pressure keeps together all the grains in the liquid phase. Both the two-body cohesion due to liquid bridges and the suction at the liquid–air interfaces play important roles in the funicular state.

It is very difficult to directly observe the liquid distribution in three-dimensional granular assemblies, though the liquid distribution should be readily observable for two-dimensional wet granular aggregates confined by Plexiglas plates (cf. [25]). As we will see later, liquid bridges in three dimensions for rather small liquid content

Table 2. Granular media with various amounts of liquid [23, 24]. In the schematic diagrams in the third column, the filled circles represent the grains and the grey regions represent the interstitial liquid.

Liquid content	State	Schematic diagram	Physical description
No	Dry		Cohesion between grains is negligible.
Small	Pendular		Liquid bridges are formed at the contact points of grains. Cohesive forces act through the liquid bridges.
Middle	Funicular		Liquid bridges around the contact points and liquid-filled pores coexist. Both give rise to cohesion between particles.
Almost saturated	Capillary		Almost all the pores are filled with the liquid, but the liquid surface forms menisci and the liquid pressure is lower than the air pressure. This suction results in a cohesive interaction between particles.
More	Slurry		The liquid pressure is equal to, or higher than, the air pressure. No cohesive interaction appears between particles.

have recently been visualized by using index matching techniques [22, 26, 27], but it seems to be difficult to extend the method for much larger liquid content. The detailed liquid distribution in the each liquid content regimes described in table 2 still remains as one of many ‘open problems’ that we list below as areas that have not been sufficiently well studied so far.

Conventionally, these liquid content regimes have been distinguished by measuring the relation between the liquid content S and the suction ΔP [23] as we will see below, where S is the ratio of the volume of liquid V_l in the system to the volume of the voids V_v in the granular media (when the total volume of the system is V_t and the volume occupied by grains is V_s , then $V_v = V_t - V_s$ and $V_v = V_l + V_a$ where V_a is the air volume in the system). Some authors define S as the percentage of the liquid content (i.e. multiplying the ratio of $S = V_l/V_v$ by 100). Here, either case (ratio or percentage) is clear from the text.

2.2.2. Liquid content and suction

2.2.2.1. Measurement of suction in granular media. There are several ways to measure the suction ΔP in granular media, and the appropriate method should be chosen regarding the measurement range of ΔP . Table 3 shows the list of methods and the range of measurements [28] commonly used in soil mechanics (where the

Table 3. List of methods to measure the suction and practical suction range for each measurement. Methods based on the osmotic pressure difference (e.g. due to gradients of solute concentration) are not listed below. Adapted from [28].

Technique or sensor	Suction range (kPa)	References
Tensiometers	0–100	[29, 30]
Axis translation techniques	0–1500	[31, 32]
Electrical or thermal conductivity sensors	0–400	[33–35]
Contact filter paper method	Entire range	[36]

mixture of soil grains and water is considered as a specimen).¹ It is beyond the scope of this brief review to describe all the experimental methods used, but these are described in the references. As examples, below we describe two often-used methods, called the axis-translation techniques and tensiometers, which make use of the capillary pressure in a porous ceramic disk to measure and control the suction [28].

Relatively low suction can be measured or controlled by using tensiometers and the axis-translation technique [28]. A schematic diagram to describe these methods is given in figure 4; these methods make use of the properties of what is called a ‘High-Air-Entry (HAE) material’, which is a material with many microscopic pores, such as a porous ceramic. In figure 4, a container is separated in two parts by a HAE disk; the bottom part of the box is filled with a liquid with pressure P_l , while the upper part is filled with air with pressure P_a . A magnified view of the HAE disk is given in the inset (a), where the pores of the HAE material are saturated with liquid. There, the surface tension at the liquid–air interfaces formed in the pores allow a finite pressure difference between the liquid and air. Considering equation (2) and the magnified view (a) in figure 4, the largest possible pressure difference between the air and liquid in the HAE material is roughly given by

$$\Delta P_{\max} = \frac{2\gamma}{R_{\max}}. \quad (5)$$

Here, as a first approximation, we assume that the pores are tube-shaped with maximum radius R_{\max} ; for smaller pore size, ΔP_{\max} would be larger. The liquid pressure P_l in the lower part of the container and the air pressure P_a in the upper part can be separately controlled without allowing the air to enter the lower part of the container, as far as $(P_a - P_l) < \Delta P_{\max}$ is satisfied.

Now, let us place a wet granular material on the HAE disk inside the container (figure 4, inset (b)) [28]. When the equilibrium is reached after a long enough waiting

¹When solutes are dissolved in water, in the soil, the osmotic effects produce the chemical potential difference from free water, where free water is the water that contains no dissolved solute, has no interactions with other phases that produce curvature to the air-water interface, and has no external force other than gravity [28]. In the soil mechanics, this chemical potential difference is sometimes measured in the unit of pressure, and it is referred to as osmotic suction. The pressure difference between the air and liquid (water) in soil $\Delta P = P_a - P_l$, which is due to capillary effect and shortrange adsorption of water to grain surfaces, is referred to as matric suction. In this paper, we focus on the latter, and ΔP is simply referred to as suction.

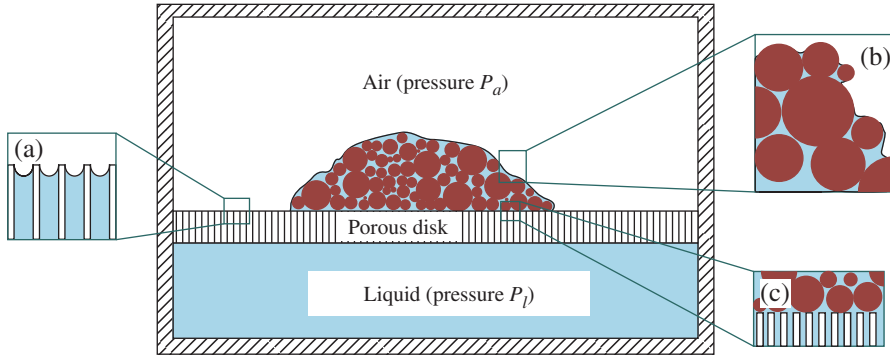


Figure 4. (colour online). Schematic diagram describing the tensiometers and the axis-translation techniques. The filled circles represent grains and the light blue region represents a liquid. The container is separated by a High-Air-Entry (HAE) porous disk that has many microscopic pores. The upper part is filled with air with pressure P_a , and the lower part is filled with liquid with pressure P_l . The pores in the porous disk are filled with liquid, and the menisci at the top surface of the pores in the porous disk (a magnified view is shown in inset (a)) make it possible to keep $P_l < P_a$. A wet granular assembly is placed on the porous disk (a magnified view is shown in inset (b)), and liquid in the wet granular media is in good contact with the liquid in the porous disk (a magnified view is shown in inset (c)); the liquid pressure around the wet grains equals the pressure P_l of the bulk liquid in the bottom of the container. Adapted from [28].

time, the liquid pressure in the wet granular medium should be equal to the liquid pressure P_l in the lower part of the container, if the liquid phase in the granular medium is in good contact with the liquid in the pores of the HAE disk (figure 4, inset (c)). The air pressure P_a and the liquid pressure P_l in the upper and lower parts of the container, respectively, can be easily measured, or even controlled, and the suction ΔP in the wet granular material is given by $\Delta P = P_a - P_l$ [28].

The method to control the suction ΔP by controlling the liquid and air pressures separately is called the axis-translation technique [28]. Initially a saturated granular material is placed on a HAE disk that separates the liquid and the air, as schematically shown in figure 4, and the liquid in the granular assembly is drained until the system reaches the equilibrium, where the liquid pressure in the granular medium becomes equal to that of the bulk liquid in the lower box. The tool to measure the suction by using the HAE disk is called a tensiometer, which is composed of a cup made of a HAE ceramic, and a sensor to measure the liquid pressure, connected by a tube filled with liquid (water) [28]. The HAE ceramic cup is placed in the wet granular assembly, and the pore pressure is measured by a direct exchange of liquid between the sensor and the wet granular medium. Note that, in using either the axis-translation technique or a tensiometer, the maximum possible value of the suction is limited by ΔP_{\max} ; other methods used to measure larger pressure differences are listed in table 3 and [28].

2.2.2.2. Relation between the liquid content and suction. The schematic description of the suction ΔP versus the liquid content S is shown in figure 5 [23, 28]. Two lines are shown because there is a hysteresis in the wetting and drying processes. In both

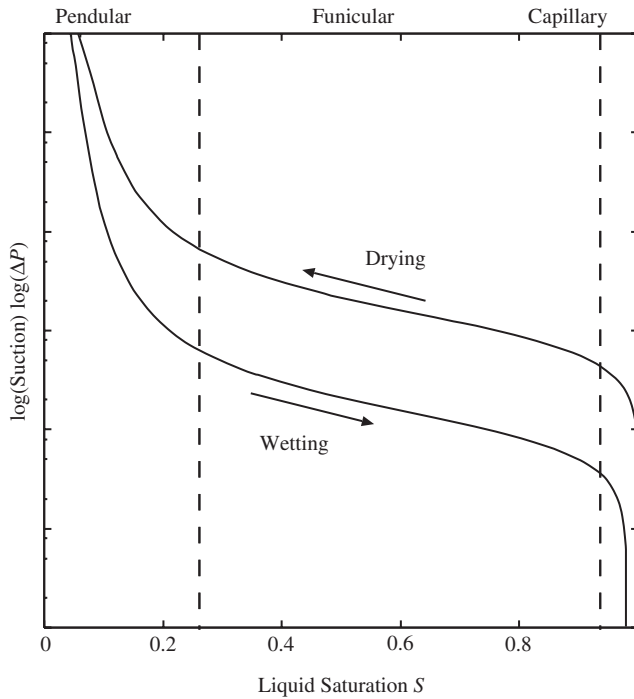


Figure 5. A schematic plot of the suction ΔP versus the liquid content S . The suction is shown in a log-scale. The upper curve represents the drying process, and the lower curve represents the wetting process. It changes the slope significantly near the phase boundaries between the pendular, funicular, and capillary states.

lines, the slope for low and large liquid content is much larger than that for intermediate liquid content. This change of slope reflects the liquid distribution in granular media.

For simplicity, let us consider the drying process (the drainage of liquid) from completely saturated granular media. At first the material is in the slurry state, and the liquid pressure is the same as or larger than the air pressure. After an appropriate amount of liquid is drained, the media is in the capillary state, and the liquid pressure becomes lower than the air pressure, i.e. the suction ΔP becomes positive. When we further decrease the liquid content S in the capillary state, ΔP increases very rapidly upon decreasing S ; ΔP is determined by the curvature of the liquid surface, and the change of the surface curvature requires little change of liquid content S because bulk liquid remains in the system. When ΔP exceeds a critical value, which is mainly determined by the surface tension and the geometry of granular media around the surface liquid, air starts to enter the bulk of the system and the funicular state is obtained. The suction still increases as the liquid content decreases, but its rate of increase becomes much smaller than that in the capillary state, because the liquid in the pores in the bulk needs to be removed. At some point, most of the voids will be filled with air, and the rest of the liquid is found around the contact points between neighbouring grains and in the liquid film that covers

the grains' surfaces. Namely, the system is in the pendular state. In this pendular state, a small change of the liquid content again results in a relatively large change of the suction, because the total amount of the liquid is much smaller than the void volume V_v , and the change of curvature at each liquid bridge requires only a small change of the liquid content S .

As shown in figure 5, for a given value of the suction ΔP , the liquid content S is smaller for the wetting process of initially dry granular media than that of the drying process of initially saturated grains. This is partly because of the hysteresis in the wetting and drying processes at solid surfaces [22, 37, 38], and partly because the variation of the pore size in the granular medium [28]. The flow of liquid in porous media (including granular media) is an important and interesting problem; indeed, this problem has developed into a separate research area. For a recent review on this problem, in terms of statistical physics, see [39].

3. Mechanical properties

In this section, we summarize what is known about the mechanical properties of wet granular media. As mentioned above, here we focus on granular cohesion in the static and quasi-static regimes for varying liquid content. To also have some idea about the dynamics, dynamical experiments are briefly presented in the final part of this section.

3.1. Granular cohesion in the static and quasi-static regimes

3.1.1. Compaction of wet granular media. The configuration of grains in a container shows history-dependence. In the case of dry granular media, the material just poured in a container is compacted when it is tapped. The dynamics of this compaction process is slow, which is known to show logarithmic dependence on the number of taps (e.g. [40–42]).

In the case of wet granular media, very low-density configurations can be realized even when the grains are spherical. Due to the cohesion, a configuration with many large openings or gaps surrounded by chains of particles can be stabilized, which may not be stable for dry spherical grains [43]. The compaction via a ram of this low-density configuration by a quasi-static compression has been examined [44, 45]. With increasing pressure on the system, the relatively large openings between particles disappear; a grain in a chain snaps in away from the chain, and the chain structure changes. After the openings disappear, a high-density region is formed, and the density difference between the initial low-density and newly formed high-density regions becomes clearly visible. One can see that the domain wall between the high-density and low-density regions travels through the system like a wave.

The realizability of very low-density structures indicates that the hysteresis of configurations in wet granular media can be stronger than that in dry granular media. In other words, the many huge gaps or openings that are possible in wet granular media, make the configuration phase space available to the grains much larger than the dry granular case (see also table 1).

3.1.2. Angle of repose for small amounts of liquid

3.1.2.1. Experiments. The angle of repose θ_r and the critical angle θ_c are measurable quantities that are sensitive to the cohesion. Here, the critical angle θ_c is the surface angle just before an avalanche occurs, while the angle of repose θ_r is the surface angle after the avalanche, and is typically slightly smaller than θ_c . When the amount of liquid is small, the cohesion is also small, but the cohesion is still detectable through θ_r and θ_c of either a granular pile or in a drum that rotates very slowly [46–51].

Even the humidity in the air is enough to induce cohesion for initially dry granular material [46, 49, 52–57]. Bocquet *et al.* [46] measured the critical angle θ_c of glass beads in humid air, and found that θ_c depends on the waiting time t_w , namely, how long they waited after preparing the sample until measurement. They reported the relation $(\tan \theta_c - \tan \theta_0) \propto \log(t_w) / \cos \theta_c$, where θ_0 is a constant (figure 6), and also found that the t_w -dependence of θ_c varies with humidity.

This time dependence of the critical angle θ_c on the waiting time t_w has been analysed based on the capillary condensation, which results from the fact that the equilibrium vapour pressure in a narrow space where non-zero suction ΔP is allowed is lower than that in the bulk [58].² Due to this effect, the vapour can condense for lower pressures in a narrow space, like the point where particles are in contact, resulting in tiny liquid bridges at the contact points between touching grains. The critical angle θ_c increases due to the cohesion from these tiny bridges, which becomes larger and increases with time because more and more vapour condenses.³

Hornbaker *et al.* [47] investigated the angle of repose θ_r of spherical polystyrene beads mixed with either corn oil or vacuum-pump oil by the draining-crater method. They measured the liquid content dependence of the angle of repose θ_r . They found that θ_r increases linearly with the average oil-layer thickness δ_{liq} (the volume of oil added divided by the total surface area of particles), indicating that the cohesion increases as the amount of liquid increases. However, as they increased the liquid content, particles started to form correlated particle clusters (clumps), and finally θ_r could not be determined in a well-defined manner. The distribution width of the measured angle of repose became suddenly wide for a certain amount

²‘Capillary condensation’ can be understood as follows; consider air and liquid in a box, where the liquid pressure p_l , the total air pressure is p_a , the liquid vapour pressure p_v , and dry air pressure $p_{\text{da}} = p_a - p_v$. From the Gibbs–Duhem equilibrium criterion and ideal gas approximation for the air, Kelvin’s equation [58] is obtained: $p_v = p_{v0} \exp[-(\Delta P v_l)/(R_g T)]$, where v_l is the partial molar volume of liquid, p_{v0} is the saturated vapour pressure, T is the absolute temperature, and R_g is the gas constant. Thus, when $\Delta P > 0$, p_v becomes smaller than p_{v0} . Namely, in narrow spaces like pores in granular media, the vapour can condense for lower vapour pressures.

³It should be noted, however, that there are alternative explanations about the origin of cohesion in this experiment. Restagno *et al.* [52] conducted similar experiments for glass beads with water and glass beads with ethanol, and found that the difference in the increase of the critical angle is larger than the value expected from the difference of the surface tension between water and ethanol. This might be partly due to the chemical reaction between silica and water [52, 59].

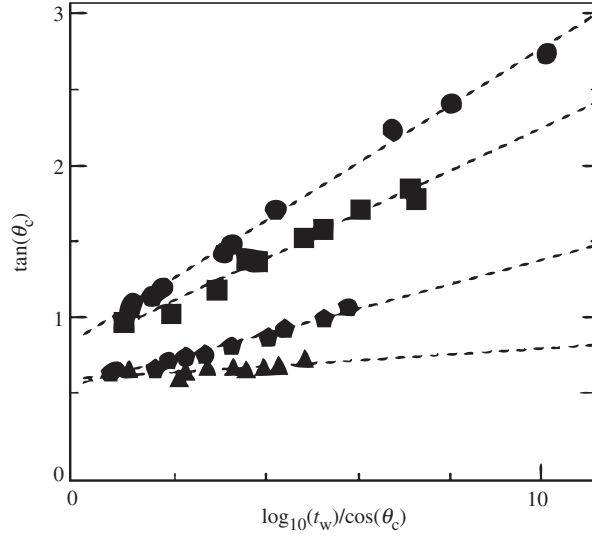


Figure 6. The critical angle θ_c of glass beads in humid air as a function of the waiting time t_w , in a slowly rotating drum, shown as $\tan \theta_c$ versus $(\log_{10} t_w / \cos \theta_c)$. The time is in units of seconds, and humidities are 15% (triangles), 27% (pentagons), 36.1% (squares), and 45.5% (circles). As time passes, more and more liquid condenses at the contact points between particles, increasing the cohesion between them. Therefore, the critical angle increases with time. From [46].

of liquid, suggesting a transition to a situation where long-range correlations dominate.

3.1.2.2. Cohesion and angle of repose. The observed increase of θ_f and θ_c with increasing liquid content should be due to the cohesive force between grains. The relation between the surface angle and cohesion, however, has not yet been clearly understood. This is an area that would greatly benefit from more systematic studies.

The most well-known analysis of the critical angle θ_c in granular engineering is to use the failure condition for a continuum description [3, 50]. In the case without cohesion, a phenomenological failure criterion for granular media is given in terms of the shear stress τ and the normal compressible stress σ as

$$\tau > \mu\sigma, \quad (6)$$

where μ is the internal friction coefficient, considered as a material parameter. If there is any plane for which the ratio τ/σ exceeds μ , the material fails at that plane; $\tau_f/\sigma_f = \mu$, where the subscript f for the stresses τ_f and σ_f indicates the value at the failure plane. The critical angle corresponds to the angle of this failure plane, where the failure starts. At the same time, because the stress comes from the weight above the plane, as schematically shown in figure 7, we have

$$\tau_f = \rho g D \sin \theta_c \quad \text{and} \quad \sigma_f = \rho g D \cos \theta_c, \quad (7)$$

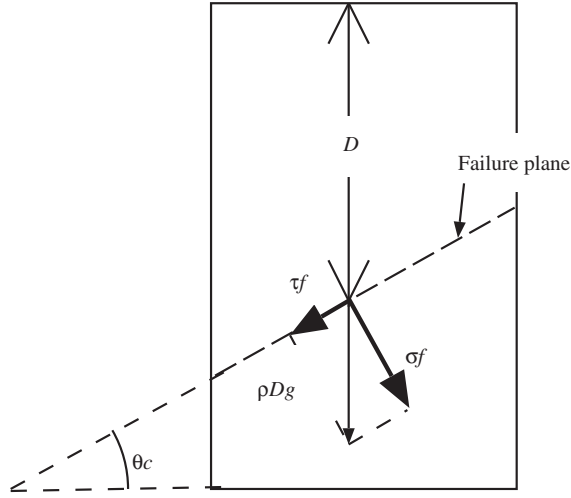


Figure 7. Schematic diagram of the force balance at the failure plane, as determined by the Mohr-Coulomb failure criterion.

with mass density ρ and the depth D of the failure plane from the surface before failure. Namely, we have

$$\frac{\tau_f}{\sigma_f} = \tan \theta_c = \mu, \quad (8)$$

which gives θ_c for dry granular media.

In the case of wet granular media, it has been considered that the cohesion result in a normal cohesive pressure σ_c [3, 50]. This additional normal stress σ_c allows to support a finite shear stress, even in the limit of zero applied normal stress σ . Then, the criterion in equation (6), for non-cohesive material, is modified into [3, 50]

$$\tau > \mu(\sigma + \sigma_c). \quad (9)$$

The criterion in equation (9) is called the Mohr-Coulomb criterion, and equation (6) is the special case of equation (9) with $\sigma_c = 0$. With non-zero σ_c , the stresses at the failure plane satisfies $\tau_f = \mu(\sigma_f + \sigma_c)$, while we still have equation (7) for the force balance. Then we have

$$\mu = \tan \theta_c \left(1 + \frac{\sigma_c}{\rho g D \cos \theta_c} \right)^{-1}, \quad (10)$$

which shows that θ_c decreases with increasing D . Namely, the criterion is the strictest at the bottom of the sandpile, which has the largest D . Therefore, the failure occurs at the bottom of the sandpile, and equation (10) with D being the total depth of the sandpile gives the critical angle θ_c of that sandpile. Note that the relation for the non-cohesive case, equation (8), is recovered in the limit of $D \rightarrow \infty$; the frictional force that holds the pile increases with the size of the pile because the normal pressure increases, but the cohesive force remains constant, thus the cohesive force becomes irrelevant in a large enough granular pile [3, 50]. We have increasing

critical angle due to cohesion only for a finite sandpile where $\sigma_c/\rho gD$ is finite, and within this range θ_c increases with the cohesive stress σ_c and depends on the pile size. Note that, in this Mohr–Coulomb criterion, the yield shear stress is the consequence of the increased normal pressure, and the direct contribution of particle–particle cohesion to the shear stress is not taken into account.

In the case of the pendular state, the cohesive stress σ_c arises from the liquid bridges between particles. Rumpf [60] proposed a simple model to estimate the cohesive stress from the force per bridge in isotropic granular media of identical spheres with diameter d , ignoring the effect of distributions in liquid bridge sizes and in number of bridges per particles [27]. He estimated the cohesive force σ_c per unit area as

$$\sigma_c \approx \nu \frac{k}{\pi d^2} F, \quad (11)$$

where ν is the packing fraction of the grains, k is the average number of liquid bridges per particle, and F is the average force per liquid bridge.⁴

According to the Rumpf model in equation (11), σ_c is proportional to the cohesion per liquid bridge F . Then, the fact that θ_r for wet spherical glass beads increases with liquid content [47] may suggest increasing F by increasing the liquid bridge volume, if the number of bridge per particle k stays constant. However, this cannot be understood by simply considering the pendular state for completely spherical beads. For the case when two spheres are in contact ($h=0$) and the wetting angle $\theta=0$, we get from equation (3) that

$$F_{\text{bridge}} = \frac{2\pi r\gamma}{1 + \tan(\phi/2)}, \quad (12)$$

where r is the radius of the spheres and ϕ is given in figure 3. Equation (15) gives $\partial F_{\text{bridge}}/\partial\phi < 0$. Namely, the attracting force F_{bridge} becomes smaller as the amount of liquid in the bridge increases, while keeping the particle separation equal to zero.

This discrepancy can be resolved by considering the surface roughness of the grains [48, 50]. It has been known that, in the case of the cone-plane contact, the attracting force increases when the amount of liquid increases [61]. If the liquid bridge volume is small enough to neglect the curvature of the macroscopic spherical shape of the beads, the surface roughness becomes more relevant, and the geometry at the contact point can be considered as the cone-plane type. If the liquid bridge becomes wide enough compared to the macroscopic curvature of the surface, then the estimation for spheres in equation (12) is expected to work.

Mason *et al.* [26] experimentally observed how the liquid distributes in spherical beads with microscopic surface roughness. They found that, when the amount of liquid is smaller than a critical value, most of the liquid is trapped on the particle surface due to the surface roughness (figure 8(a)) and the critical angle did not depend on the surface tension of the liquid. When the liquid content exceeds a critical

⁴In papers on granular engineering including [60], the porosity n defined as the ratio of the void volume V_v to the total volume V_t is often used instead of the packing fraction ν as a parameter to characterize the packing. These parameters are related by $n = 1 - \nu$.

value, liquid bridges are formed at the contact points (figure 8(b)), and the critical angle increases with liquid volume and depends on the liquid surface tension. This agrees with the behaviour expected from the regime where the surface roughness determines the cohesion from a liquid bridge.

However, one should note that, not only the cohesion force F , but also the number of liquid bridges k per particles depends on the liquid content in general, which should also affect the cohesive stress σ_c . Recent experiments [27, 62] show that k increase very rapidly upon liquid content for small liquid content, and then saturate. The effect of k on the critical angle needs to be investigated carefully especially for small liquid content.

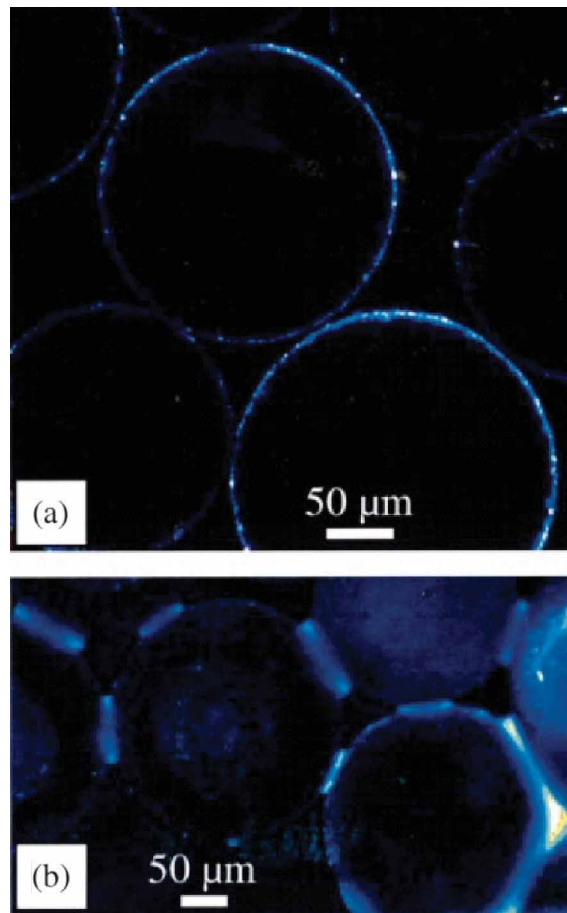


Figure 8. (colour online). Distribution of small amount of liquid in granular media. The blue region shows the location of the liquid. The average grain diameter is $240\ \mu\text{m}$. (a) When the amount of liquid is small, the liquid is uniformly distributed at the grain surface. (b) When the amount of liquid is large enough, most of the liquid is caught at the contact points between particles and liquid bridges are formed. From [26].

Albert *et al.* [48] proposed a criterion to understand the critical angle different from the Mohr–Coulomb criterion. They considered the criterion whether a grain at the surface escapes from the bumpy geometry that other grains form. In their theory, the surface grain at an unstable position rolls down and the final angle is determined by the condition that all grains at the surface sit at stable positions. The cohesion from liquid affects the force balance and increases the critical angle θ_c .

In either mechanism, the Mohr–Coulomb criterion or the surface failure criterion, the angle of repose of cohesive granular media is larger than that of non-cohesive granular media. However, the location of the failure plane is different. The failure occurs at the bottom in the case of the Mohr–Coulomb criterion and θ_c depends on the system size, while the surface fails for the ‘grain escape’ criterion and θ_c is independent of the system size. In addition, the Mohr–Coulomb criterion is a continuous description, while the grain escape criterion explicitly considers the discreteness of the system.

Both mechanisms may be responsible in determining the critical angle. However, it is likely that the discrete picture is dominant for very small amounts of liquid content, with small cohesive bulk stress, while the continuous picture is appropriate when the liquid content is enough to cause the cohesive bulk stress comparable to gravity. In order to see the relevant mechanism, Tegzes *et al.* [63] examined the system size dependence of the angle of repose θ_r for a larger range of liquid content (figure 9). They adopted the draining crater method, and the system size is controlled by changing cylinder diameters. They found that θ_r is independent of system size for small enough liquid content (called the *granular regime*, where surface flow occurs at the top few layers), while it decreases with system size for larger liquid content (called the *correlated regime*, where grains form clumps and the surface flow is correlated). At the largest liquid content, the angle first decreases and then increases slightly with oil-layer thickness, but still depends on the system size (called the *plastic regime*, where the medium retains a smooth crater surface and the motion is coherent). Qualitative agreements have been obtained with the surface failure criterion for the granular regime and with the Mohr–Coulomb criterion for the correlated and plastic regime.

These results are not yet conclusive, and many researches on the surface angle are still going on. Ertas *et al.* [64] considered the critical angle in a pile made of a mixture of spheres and dumbbell-shape grains, extending the surface failure criterion by [48]. They found that the surface angle drastically increases as the fraction of dumbbell-shape grains increases, because the dumbbell-shape grains hardly roll down the slope. They pointed out that, in wet granular media with small liquid content, liquid bridges connect a few grains and make clumps; these clumps may contribute to the increasing surface angle through the same mechanism that the fraction of dumbbell-shaped grains increased the critical angle. On the other hand, Nowak *et al.* [65] applied the geometrical consideration of force balance by [48] not only at the surface but also inside the material. They claimed that the most unstable plane from the geometrical consideration is inside the material. Their argument does not take into account the effect of friction, but it gives system-size dependent critical angle that agree with the critical angle of dry grains in the limit of infinite system size; this feature is similar to that in the Mohr–Coulomb criterion.

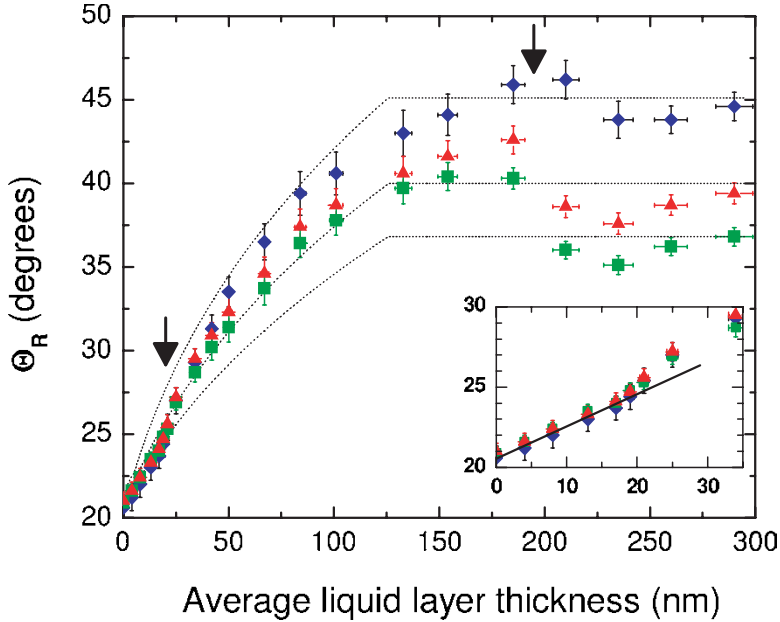


Figure 9. (colour online). Angle of repose θ_r versus the average oil-layer thickness δ_{liq} for spherical glass beads with average diameter 0.9 mm with three different container diameters d_c (diamonds: 10.3 cm, triangles: 15.6 cm, squares: 20.4 cm). The inset shows an enlargement of small δ_{liq} regime. The two vertical arrows indicate the transitions between the granular, correlated, and plastic regime. From [63].

In summary, the effect of cohesion on surface angle in granular pile has not yet been clearly understood, and further systematic studies are needed.

3.1.3. Tensile, compression, and shear tests for intermediate and large liquid content. For large enough cohesion, the angle of repose may exceed 90° for laboratory-scale granular piles. In such a regime, the angle of repose is no longer a good parameter to characterize the cohesion, and we need another method to characterize the cohesion in wet granular media.

If the failure condition is characterized by the Mohr–Coulomb criterion (9), the measurement of the stresses at the failure gives the cohesive stress σ_c , which characterizes the cohesion in wet granular media. The analysis of granular media based on the Mohr–Coulomb criterion has been well-established in the engineering field, and a considerable amount of data has been accumulated for wet granular media. In this subsection, we briefly describe several experimental methods to determine the internal friction coefficient μ and the cohesive stress σ_c , and summarize what has been known for wet granular media from those measurements.

3.1.3.1. Test methods and Mohr circle. Several experimental methods have been used to measure the tensile strength of wet granular media (e.g. [66, 67]). The simplest method is just to pull the sample apart until the material fails, as shown in figures 10(a) and (b). However, it is difficult to hold the sample because wet granular media are fragile and not always uniform. In the adhesive method

(figure 10(a)), the material needs to be strong enough so that the bottom and top faces of the sample can be bonded to the adaptors. In the case of the split-plate method (figure 10(b)), the sample is placed on a plate, and the plate is split until the material fails. In either method, both the stress and the strain can be measured until reaching failure.

The uniaxial and diametrical compression tests have also been conducted, where the sample is compressed in one direction until it fails. In uniaxial compression tests (figure 10(c)), a sample is pressed by a ram along one direction. In the case of the diametrical compression test, a linear load is applied to a sample of cylindrical shape across one diameter of the disk (figure 10(d)), and the tensile stress is calculated based on the Hertz theory for isotropic elastic bodies [68, 69], though the validity of the elastic theory for granular media with the assumption of the isotropy is rather suspicious.

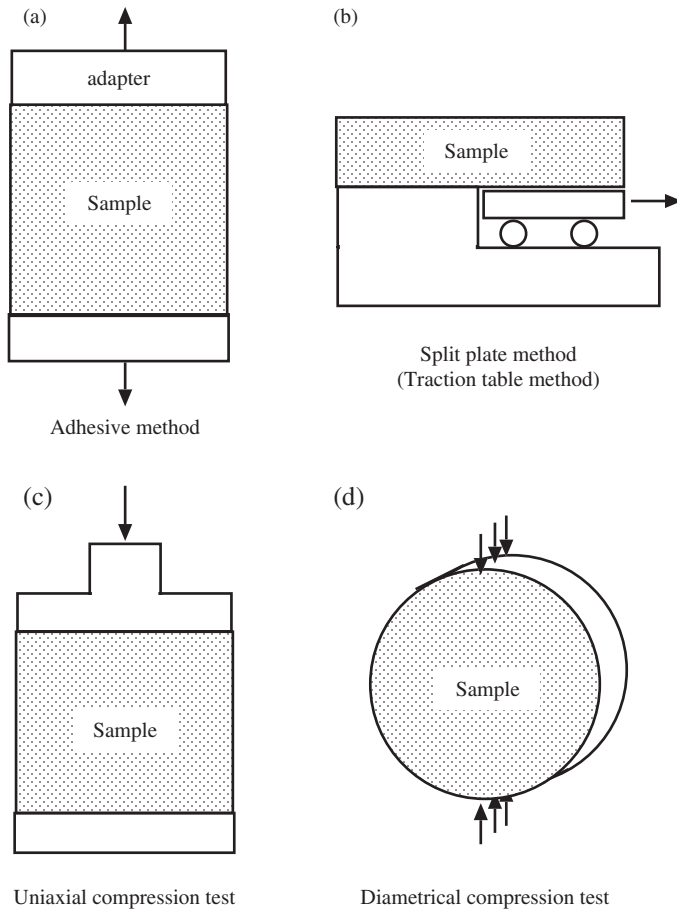


Figure 10. Several measurement techniques of strength of granular media. (a) the adhesive method, (b) the split-plate method (traction table method), (c) the uniaxial compression test, (d) the diametrical compression test.

In addition to these uniaxial tests, where only one component of the stress applied to the sample is controlled, there are methods where two components of the stress are separately controlled. The triaxial compression test has been widely performed for soils [28, 70, 71]. Figure 11(a) shows a schematic description of the triaxial testing system. The cylindrical-shaped sample is placed in a confining cell filled with fluid, and the sample is separated from the confining fluid by a flexible membrane. The sample is compressed from above by a ram, and the pressure at side membrane can be separately controlled by changing the pressure of the confining fluid. In the case of the direct shear test in figure 11(b), a sample in a shear box is sheared as the shear box is slid. A series of tests can be conducted by varying the vertical compressive stress from the top. Note that there are several modifications of these tests; in the case of unsaturated soils, the modified tests are often performed, where the suction is kept constant during the test by using the HAE material (see subsection) and allows the liquid to drain from the sample [28].

It should be noted that the sample needs to be prepared carefully in either method in order to get reproducible results. Especially, how the sample is compacted before the measurement is an important factor to determine its mechanical response.

The results of the tensile, compression, and shear tests are often analysed by using the Mohr circle, which visualizes the rotational transformation of the two-dimensional stress tensor as follows [28, 70, 71]. Let us consider a two-dimensional stress tensor whose principal values are σ_1 and σ_2 . If the coordinate axes are rotated by an angle α from the principal axes, the stress tensor σ_{ij} in the coordinate system is given by

$$\begin{pmatrix} \sigma_{11} & \sigma_{12} \\ \sigma_{21} & \sigma_{21} \end{pmatrix} = \begin{pmatrix} \cos \alpha & \sin \alpha \\ -\sin \alpha & \cos \alpha \end{pmatrix} \begin{pmatrix} \sigma_1 & 0 \\ 0 & \sigma_2 \end{pmatrix} \begin{pmatrix} \cos \alpha & -\sin \alpha \\ \sin \alpha & \cos \alpha \end{pmatrix} \\ = \begin{pmatrix} \frac{(\sigma_1 + \sigma_2)}{2} + \frac{(\sigma_1 - \sigma_2)}{2} \cos 2\alpha & \frac{(\sigma_1 - \sigma_2)}{2} \sin 2\alpha \\ \frac{(\sigma_1 - \sigma_2)}{2} \sin 2\alpha & \frac{(\sigma_1 + \sigma_2)}{2} - \frac{(\sigma_1 - \sigma_2)}{2} \cos 2\alpha \end{pmatrix} \quad (13)$$

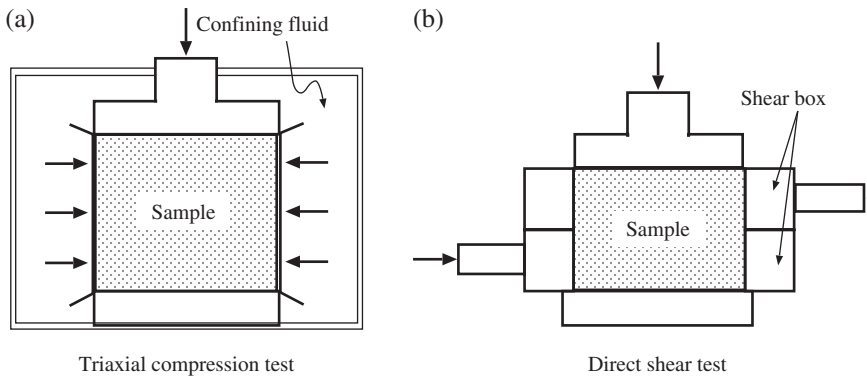


Figure 11. Schematic diagrams; (a) a triaxial test system, (b) a direct shear test system.

Namely, when we consider two points $A(\sigma_{11}, \sigma_{12})$ and $B(\sigma_{22}, -\sigma_{21})$ in the $\tau - \sigma$ plane, they locate at the diametrically opposed points on a circle

$$\left[\sigma - \frac{1}{2}(\sigma_1 + \sigma_2) \right]^2 + \tau^2 = \left[\frac{1}{2}(\sigma_1 - \sigma_2) \right]^2, \quad (14)$$

as shown in figure 12, where the angle between the σ axis and the line $A - B$ is 2α .

The Mohr circle is useful when considering the Mohr–Coulomb criterion (9). The stress at failure, from the Mohr–Coulomb criterion, gives a straight line

$$\tau = \mu(\sigma + \sigma_c) \quad (15)$$

in the $\tau - \sigma$ plane with σ -intercept at $-\sigma_c$ and slope μ . Instead of μ , $\Phi = \tan^{-1} \mu$ (shown in figure 12) is also used as a parameter for the Mohr–Coulomb criterion; Φ is called the internal friction angle. If the granular aggregate obeys the Mohr–Coulomb criterion, the Mohr circle at failure should be tangent to this straight line (15), because the granular aggregate fails as soon as a stress state that satisfies the criterion appears. Therefore, by drawing an envelope curve of Mohr circles at failure with various stress conditions, from the data one can construct the Mohr–Coulomb criterion to determine the parameters μ and σ_c .

This procedure can be done for the triaxial compression test and the shear test, where two components of the stress tensor are varied separately. The granular material does not always follow the ideal Mohr–Coulomb criterion and the envelope might be curved, but the response is linear for small enough values of the stress, and this gives μ and σ_c .

In the case of uniaxial tensile (compression) tests, one of the principal values is always zero. Thus, the resulting Mohr circle crosses the origin of the $\sigma - \tau$ plane, where

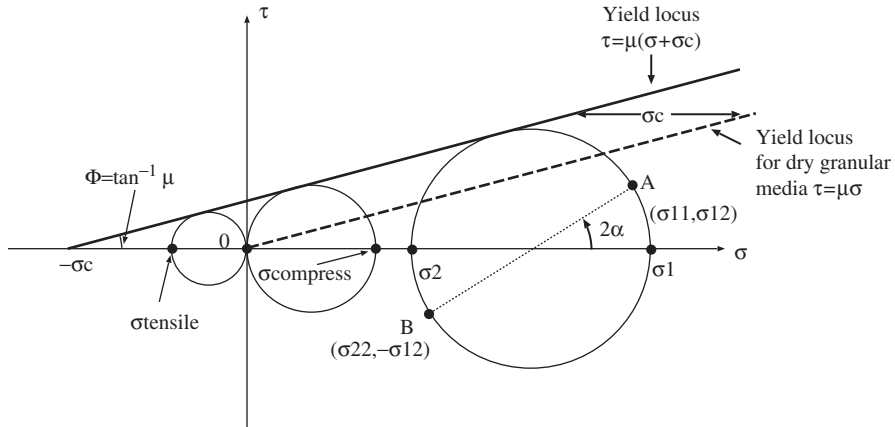


Figure 12. A schematic diagram of Mohr circles in the plane shear stress τ versus normal compressive stress σ . When a two-dimensional stress tensor (whose (i, j) component is given by σ_{ij}) is considered, the Mohr circle includes the diametrically-opposed points $A(\sigma_{11}, \sigma_{12})$ and $B(\sigma_{22}, -\sigma_{12})$, as shown in the figure. The yield locus from the Mohr–Coulomb criterion for cohesive granular media is shown by the solid straight line, and the yield locus of the non-cohesive granular media is shown by the dashed line.

the tensile (compressive) stress at failure is given by σ_{tensile} (σ_{compress}) as shown in figure 12. For a given internal friction coefficient μ , σ_{tensile} (σ_{compress}) is proportional to σ_c , and the behaviour of σ_{tensile} (σ_{compress}) gives information about the cohesion in the wet granular medium. However, we cannot determine the cohesive stress σ_c from a uniaxial test unless we know μ from another experiment.

Below let us briefly review some experimental results about the stresses at the failure state for wet granular media with various liquid content.

3.1.3.2. Tests in the pendular state. Pierrat *et al.* [72] investigated the Mohr–Coulomb criterion by using direct shear tests for various granular assemblies including monodisperse glass beads and polydisperse crushed limestone with relatively small liquid content. The amount of liquid was larger than that in the experiments on the angle of repose presented in subsection 3.1.2, but the system was supposed to be still in the pendular state.

The yield loci in shear test for glass beads of diameter $93\ \mu\text{m}$ with various liquid content are shown in figure 13, which shows a shift of the yield locus to the left from the dry case, but the slope is unchanged. It has also been found that the shift increases with the liquid content. For all the materials they investigated, they found that the yield loci can be collapsed by shifting the curve. In this experiment, the main effect of the liquid appears in the cohesive stress σ_c , but the internal friction coefficient μ was not significantly modified, which indicates that the effect of lubrication was small.

They also investigated the relation between the shear test and the uniaxial tensile test. They had conducted tensile tests separately [73], and from their empirical relation between σ_{tensile} and parameters that characterize the sample, such as packing fraction and liquid content, they estimated the tensile strength σ_{tensile} for the sample in the shear tests. If the internal friction coefficient $\mu = \tan \Phi$ for dry samples

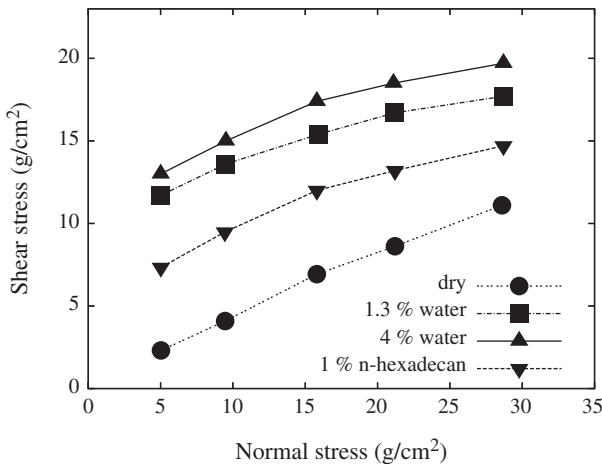


Figure 13. Yield locus obtained by direct shear tests for glass beads ($93\ \mu\text{m}$): dry (circles), with water (1.3% of liquid content is shown by squares, and 4% of liquid content is shown by triangles), and with n-hexadecan (liquid content 1%, shown by upside-down triangles). Adapted from [72].

does not change for wet granular materials, we can estimate σ_c from σ_{tensile} , using the relation $\sigma_c = (1 + \sin \Phi)|\sigma_{\text{tensile}}|/(2 \sin \Phi)$ (see figure 12) with Φ being the internal friction angle in the dry case. This estimation was compared with observed yield loci in shear tests, and reasonable agreement was found.

3.1.3.3. Tests with intermediate liquid content. Next, we review the tensile tests and uniaxial compression tests of wet granular media with intermediate liquid content, typically in the funicular state. The mechanical response of the funicular state is not well understood, because in this state even the qualitative dependence of the tensile strength (tensile stress at the peak of stress–strain relation) on liquid content varies from one material to another, and the reason for this is not very clear. Here we summarize a few experiments.

In the field of agglomeration processing, experiments have been conducted from relatively dry to almost saturated conditions. However, in the funicular state, the liquid content dependence of the strength may either increase or decrease upon increasing the liquid content. For example, increasing tensile strength with increasing liquid content has been found by Schubert [74] for limestone with mean diameter $65 \mu\text{m}$ using the adhesive method. Figure 14 shows the stress–strain relation for various liquid content S , and the peak stress gives tensile strength. Stress–strain curves, showing decreasing strength as the liquid content S increases from 36% to 70% are shown in figure 15, from [75], where compressive tests were performed using dicalcium phosphate with diameter $21 \mu\text{m}$. Kristensen *et al.* [76] found increasing strength for increasing liquid content using glass beads of particle size $68 \mu\text{m}$, while decreasing strength for dicalcium phosphate of particle size $14 \mu\text{m}$ in uniaxial compression tests. There have been many other experiments probing the mechanical strength of wet granular media (see [24] for a review). The effect of particle size on

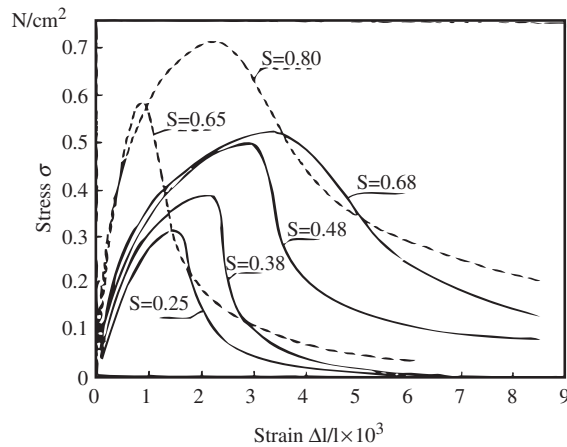


Figure 14. Stress–strain relation of wet limestone (mean diameter $65 \mu\text{m}$) obtained by the adhesive method [74]. The packing fraction ν of the sample was 0.66. The dashed lines show the result for a sample prepared by a drying process (drainage), while the solid lines show the result for a sample prepared by a wetting process (imbibition). S refers to the percentage liquid content. From [74].

the competition between cohesion and lubrication was considered [24] to be one of the causes of these various behaviours, but the liquid content dependence in the intermediate liquid-content regime (approximately given by $20\% \lesssim S \lesssim 90\%$) is not yet well-understood.

It has been found that the critical strain ϵ_c (strain at the peak in the stress–strain curve) always increases with increasing liquid content, as shown in figures 14 and 15. This indicates that the wet granular material is brittle when the amount of liquid is small, and tends to show viscoplastic behaviour as the liquid content is increased.

It should be also noted that, even for similar amounts of liquid content, the strength of a sample may depend on whether it is prepared by either draining or adding liquid; Schubert [74] found different stress–strain curves for each processes as shown in figure 14. In many studies, the sample is often driven by an external force (e.g. rotating drum, mixing, etc.) before the measurement, in order to better distribute the liquid, which would make hysteresis less obvious.

3.1.3.4. Tests in soil mechanics: relatively large amounts of liquid. As pointed out in subsection 2.2.1, the suction in the capillary state largely varies upon a small change of liquid content. In soil mechanics, the shear tests of unsaturated soils have been conducted by decreasing the water content from initially saturated soils; in other words, by increasing the suction from zero. The data is usually presented in terms of the suction ΔP , not the liquid content S . This is a reasonable way of arranging data in the capillary state, because the change of ΔP upon changing S is very rapid for low and high liquid content as has been shown in subsection 2.2.1. Here we summarize these data to try to understand the mechanical properties with large amount of liquid content. It should be noted that the grains that form soils can be very small (for example, clay can be the order of $2\ \mu\text{m}$ in diameter),

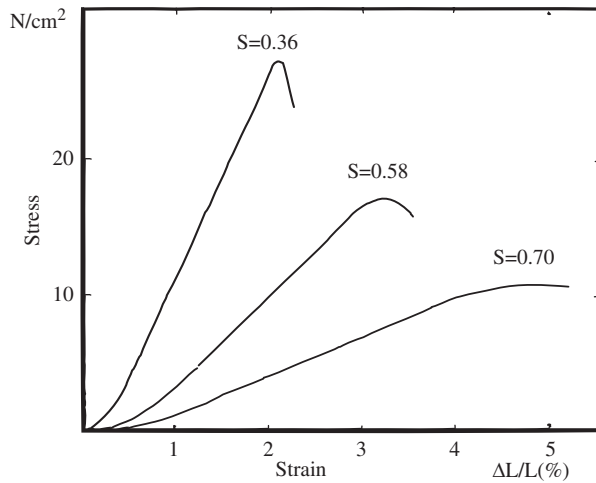


Figure 15. Stress–strain relation of dicalcium phosphate (diameter $21\ \mu\text{m}$) with an aqueous solution of a polymer. S refers to the percentage liquid content. The packing fraction of the sample was 0.5. From [75].

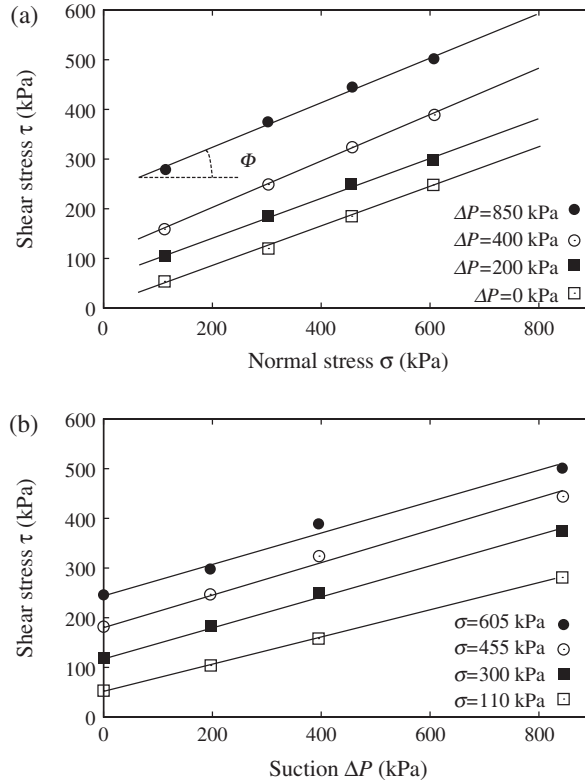


Figure 16. Yield loci for wet soil (Madrid Gray Clay). (a) Net normal stress σ versus shear stress τ for various suction $\Delta P = P_a - P_1$. The slope is almost independent of suction in this regime. (b) Shear stress versus suction for various net normal stresses σ . The slope is almost independent of the net normal stress in this regime. Adapted from [28]. (Original data from [77].)

may have characteristic shape, and may be affected by, e.g. electrostatic interaction. These properties affect its mechanical responses, but we focus on the variation of the mechanical properties upon changing the suction ΔP in the following, so that we will be able to extract the properties mainly determined by the capillary effect.

The failure condition given by the Mohr–Coulomb criterion in equation (9) has been experimentally investigated for soils. Figure 16(a) shows⁵ the yield loci of wet clay for various values of the suction ΔP , where the slope gives the friction

⁵In soil mechanics, the total normal stress σ_t , the air pressure P_a , and the water pressure P_1 are often taken to be the control parameters. Here, the total normal stress σ_t includes both the load on the granular sample and the fluid pressure on it, thus $\sigma_t = P_a$ if the sample is placed in air without any external load. When an external pressure is applied on the sample, the net normal stress σ sustained by granular particles would be given by $\sigma_t - P_a$. In the original figures of figure 16(a), the label of the horizontal axis shows ‘Net Normal Stress $\sigma - u_a$ (kPa)’, where σ in [28] represents the total normal stress, and u_a is the air pressure (σ_t and P_a in our notation, respectively).

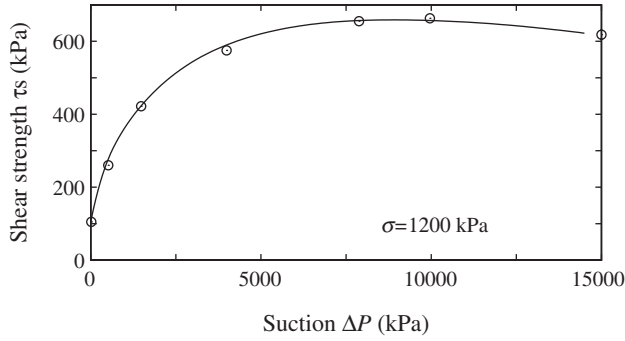


Figure 17. Shear strength τ_s versus suction ΔP obtained by shear tests for red clay. This figure shows a larger range of suction ΔP (compared to Fig. 16(b)), as well as a non-linear and non-monotonic behaviour. Adapted from [78].

coefficient μ and the y -intercepts of lines give $\mu\sigma_c$. The slopes scarcely vary with suction, which indicates that μ (the internal friction angle $\Phi = \tan^{-1} \mu$) does not depend on the suction ΔP . The y -intercept is small for $\Delta P = 0$ and increases with increasing the suction ΔP . Namely, σ_c increases with increasing ΔP .

Figure 16(b) shows the yield shear stress versus suction for various normal compressive stresses, which shows a linear dependence on ΔP . This result and the fact that the internal friction angle Φ depends little on the suction ΔP suggest that the cohesive stress σ_c increases linearly with ΔP . The linear increase of σ_c upon increasing ΔP for small ΔP is natural, because the compressive stress ΔP at the liquid–air interface at the surface of the granular assembly is the source of the cohesion. This behaviour has been found for some kinds of clay [77–79], undisturbed decomposed granite [80], silt [81], and glacial till [82].

When ΔP is increased further, a non-linear dependence of the shear strength τ_s (the shear stress at failure for a given suction and normal load) on ΔP is found [28, 78], as shown in figure 17. The increase of the shear strength τ_s becomes nearly zero as ΔP grows. It is very likely that the internal friction coefficient μ does not vary significantly upon changing ΔP in these regimes, and then the obtained shear strength τ_s is proportional to the cohesive stress σ_c .

Summarizing these results, σ_c increases linearly with ΔP for small enough suction ΔP , but for large ΔP , the increase disappears. The suction ΔP increases as the liquid content S decreases as shown in figure 5, therefore, σ_c increases upon decreasing the liquid content from $S = 100\%$ ($\Delta P = 0$) [83].

3.2. Dynamical behaviour

In this subsection, we briefly describe some dynamical behaviour of wet granular media. In the dynamical regime, not only cohesion but also other effects of the liquid such as viscosity, lubrication, and liquid motion play important roles. The dynamical behaviour observed is far more complicated than that in the quasi-static regime. In addition, though there are numerous studies of the dynamics of partially wet granular media from the practical point of view, systematic studies in simple situations

are rather few; here we briefly summarize some of the experimental studies on the dynamical response of wet granular media. Those who are interested in recent studies on dynamics should also refer to a recent review [22].

3.2.1. Dynamics in the pendular state

3.2.1.1. Avalanches in rotating drums. Granular flow and avalanches in a rotating drum have been widely investigated for dry granular media (see, e.g. [85–92]). At low rotation rate, the grains stay at rest until the surface angle reaches the critical angle θ_c , and avalanche occurs; the angle just after the avalanche is the angle of repose θ_r . This is called the intermittent regime. When the rotation rate is high enough, the continuous flow occurs with keeping a constant angle between the surface and horizontal plane; this is the continuous regime. The flow regimes of fine cohesive powders in a rotating drum has been also studied by [93].

Tegzes *et al.* [84, 94] investigated the flow behaviour of wet granular materials in a thin rotating drum. In the experiments, the amount of liquid is small (liquid content varied from 0.001% to 5%), where the pendular state is expected. They have observed the transition from intermittent to continuous flow with increasing the rotation rate in this range of liquid content.

They observed the time evolution of the surface profile, which enable them to calculate the mean surface angle, statistics of the local surface angle, evolution of pattern at the surface, etc. In figure 18, the typical surface profiles just after avalanches in the intermittent flow regime are shown. For enhanced clarity, the grey-scale plot in the third dimension of the figure shows the local surface angles.

By changing the liquid content, the following three regimes have been distinguished. For low liquid content, the cohesion is small, and small avalanches are observed (the *granular regime*); the avalanches occur at the surface and the surface profile is always smooth (figure 18, liquid content 0.04%), similarly to the dry granular media (figure 18, dry case). When increasing the liquid content, the cohesion becomes stronger, and grains move as a connected block. An avalanche occurs

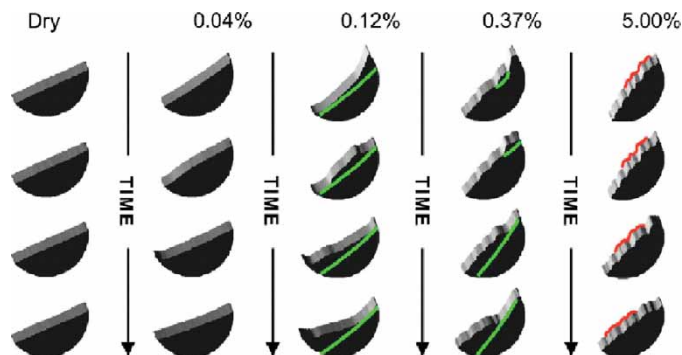


Figure 18. (colour online). Surface shapes in a rotating drum during single avalanches, for various liquid contents S (shown as percentages). The coloured line for liquid content percentages 0.12% and 0.37% indicate approximate slip planes in the correlated regime, and the coloured lines for 5.00% show the travelling quasiperiodic surface features in the viscoplastic regime. From [84].

through a succession of local slip events, and the surface structure fluctuates after each avalanche; this is the *correlated* regime (figure 18, liquid content 0.12% and 0.37%). Further increasing the liquid content results in the *viscoplastic* regime. In this state, the flow becomes coherent over the entire sample, and fluctuations are suppressed (figure 18, liquid content 5%).

They also found that the critical angle θ_c depends not only on the liquid content but also on the rotation rate. They varied the duration between avalanches, or the ‘waiting time’, from about 0.1 s to 1000 s. It was found that θ_c increased logarithmically with the waiting time. They supposed that this was caused by the slow flow of liquid along the particle surface.

A systematic study of liquid motion in wet granular media in the pendular state was recently conducted by [62]. They found that, just after shaking the material to mix the liquid with grains, the average liquid bridge volume was much less than that in equilibrium; the volume saturated after long enough waiting times, more than one hour. This also suggests that the liquid-moving process is very slow and may induce the ageing effect observed by [84, 94].

3.2.1.2. Vibrated wet granular media. Dry granular media placed on a horizontal plane excited by vertical vibrations is a fundamental and widely used set-up to study granular gases (e.g. [95]), segregation (e.g. [96]), and pattern formation (e.g. [97]). In dry granular media, the onset of fluidization is often characterized by the dimensionless acceleration $\Gamma = A\omega^2/g$, where A is the amplitude of the vibration, ω is the angular frequency of the vibration, and g is the acceleration of gravity. There is a threshold Γ_{\min} below which there are no fluidization, which was reported to be a constant around one, (e.g. [1, 98, 99]), but recently reported that Γ_{\min} can be smaller than one and show weak ω dependence [100, 101]. Above the fluidization threshold, dry granular media exhibits transitions between localized patterns of jumping grains (in the case of few layers of grains) all the way to gas-like phases (see, e.g. [102–108]).

For wet granular media, the cohesion force introduces an additional force or energy scale. It is non-trivial to determine which parameters would better characterize the resulting behaviour. Recently, experiments on this subject have been conducted [27, 109], where fluidization of glass beads wet by water under vertical vibration has been investigated. The critical dimensionless acceleration Γ_{crit} for fluidization is found to depend on the frequency $f = \omega/2\pi$, the particle radius R , and the liquid content W defined as the ratio of the liquid volume to the total volume, as shown in figure 19. Here, W is defined as the ratio of the liquid volume to the total volume. They [27, 109] found that Γ_{crit} depends weakly on f , but becomes constant for sufficiently high frequency. In this high frequency regime [27, 109], Γ_{crit} is smaller for larger R for a given W (figure 19a), while it increases with W for a given R (figure 19(b)).

Geromichalos *et al.* [27, 109] interpreted their results by considering the cohesion force due to liquid bridges between grains as well as between grains and the container wall. The increase of Γ_{crit} with W was found [109] to be proportional to the increase of the cohesion force F_{bridge} per liquid bridge, which they estimated from W . It is natural that Γ_{crit} increases with increasing F_{bridge} , but Geromichalos *et al.* [27, 109] found that the proportionality is not trivial; another possibility is that Γ_{crit} is ruled by the energy required to break the bridge, whose dependence on W should be different

from the dependence of the force. In the case of the dependence upon R , Geromichalos *et al.* [27, 109] explained it by considering the shear stress due to the formation of liquid bridges between grains and side walls; the bulk material tends to move together due to the cohesion, but if the shear from the side wall is large enough, the shear stress makes it possible to deform the bulk sample and to induce the fluidization. Following their interpretation, the decrease of Γ_{crit} upon increasing R is because the force per bridge is proportional to R but the number of liquid bridges per area is proportional to $1/R^2$, which gives the shear stress proportional to $1/R$. They [27, 109] also studied the fluidization with the container whose walls are covered by the hydrophobic material so that liquid bridges cannot

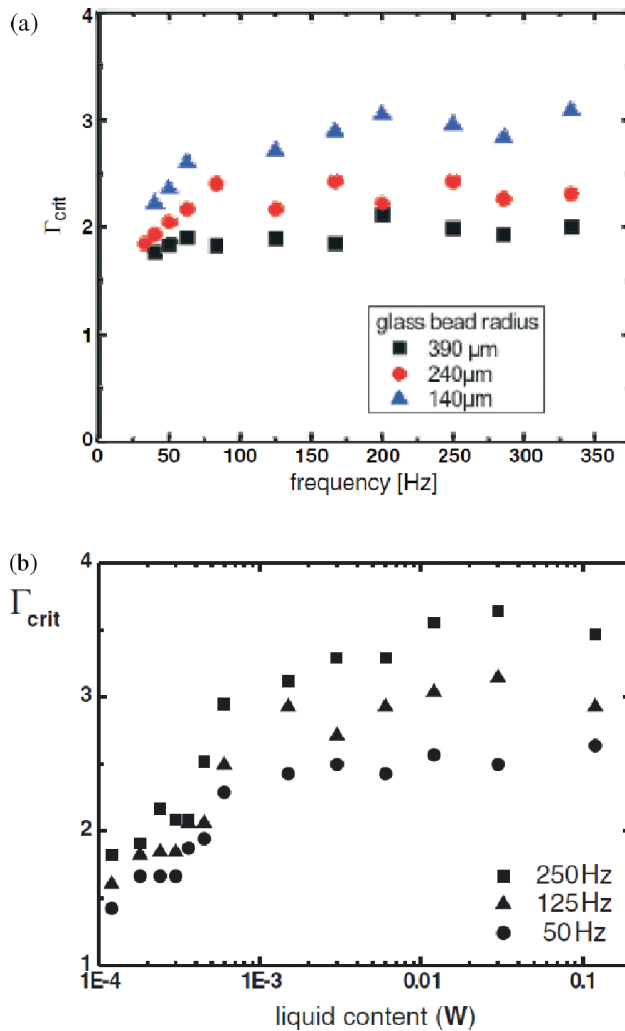


Figure 19. (colour online). (a) Critical acceleration Γ_{crit} versus frequency f for three different bead radii, with water content $W=0.5\%$. (b) Γ_{crit} versus liquid content W for three different frequencies. The particle radius R is $140\ \mu\text{m}$. From [27].

be formed with the side walls, and they found that the material cannot be fluidized up to $\Gamma = 20$.

3.2.1.3. Segregation. Segregation of grains by their size is one of the most striking phenomena of granular materials. The most well-known example is the Brazil-nuts effect, i.e. the large Brazil nuts always appear on top of mixed-nuts containers. After two or more kinds of grains are mixed together, size segregation occurs very easily when they are excited by an external energy input in, e.g. a vibrated container or chute flows. Size-segregation has been studied for dry granular material for various types of mixtures and excitations (e.g. [96, 110–112]). In wet granular materials, the cohesion tends to suppress the segregation by sticking grains together, but at the same time, various factors come into play in such a dynamical situation, as we will see below.

The size-segregation in wet granular materials that flow down an inclined plane has been investigated in [113, 114]. They used binary mixtures of glass beads with several sets of diameters. Also water, glycerol, and other kinds of liquid were used to observe the effect of the viscosity as well as the surface tension. They found that segregation is basically suppressed by increasing the liquid content, which is natural because the cohesion tends to suppress the particles' relative motion.

Samadani and Kudrolli [113, 114] investigated the phase diagrams of segregation in the space of particle diameter ratio and liquid content. These found a qualitative difference of phase diagrams between water and glycerol; the surface tensions are almost the same for these two kinds of liquid, but the viscosities are different, and the segregation is lower at higher viscosity. This is because [113, 114] viscosity tends to reduce the velocity fluctuations required for segregation.

Samadani and Kudrolli [113, 114] estimated the viscous force between moving particles connected by a liquid bridge by using the Reynolds lubrication theory, in which the hydrodynamic effect in thin space is taken into account [15, 16, 115, 116]. There [113, 114], the force is proportional to the relative velocity between moving particles, and they found that the viscous force can be comparable with the cohesive force for the characteristic velocity scale under gravity. This also suggests that the viscosity is very important for dynamical behaviour like segregation.

On the other hand, Geromichalos *et al.* [22, 117] investigated size segregation in granular media in a jar driven by a horizontal circular motion (figure 20(a)). They found that segregation sometimes occurs partially, and they investigated the degree of segregation by measuring the fraction of the mixture zone (i.e. the region where no segregation occurs) to the total sample. From the experiments, they distinguished three regimes (figure 20(b)); the *gaseous* regime, where an increase of the liquid content enhances size-segregation; the *intermediate* regime, where segregation occurs, but increasing the liquid content suppresses segregation; and the *viscoplastic* regime, where no segregation occurs. By increasing the liquid content with a fixed ratio of radii, the system state evolves from gaseous, intermediate, to the viscoplastic regimes.

The behaviour in the gaseous regime found in [117], where segregation is enhanced by increasing liquid content, seems to contradict the results in [113, 114]. Geromichalos *et al.* [117] discussed that, in the gaseous regime, the energy dissipation is enhanced by the breakage of a number of tiny liquid bridges, while the cohesion is not enough to strongly affect the dynamics. The larger energy

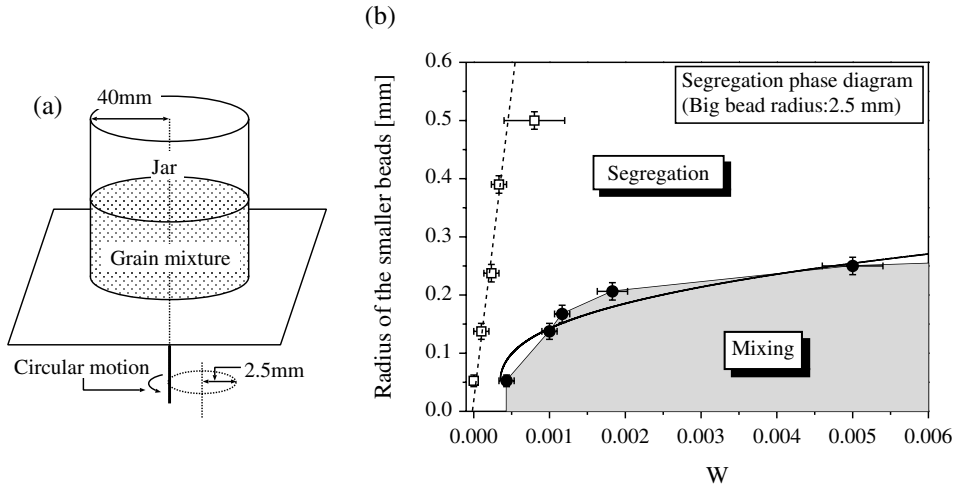


Figure 20. (a) Schematic description of the experimental setup in [22, 117]. The jar experience rapid, horizontal circular motions (20 revolutions per second), where the centre of the jar follows a small circle as shown in the figure (The jar itself is not spinning around its centre). (b) Particle-size segregation phase diagram for binary mixtures of wet granular materials. The radius of the bigger beads is fixed, and the vertical axis shows the radius of the smaller beads. The horizontal axis shows the amount of liquid via the dimensionless quantity W , defined as the volume of the liquid divided by the total volume of the small beads (including the space between the beads). The segregation does not occur in grey region. The dashed steep line separates the region where the segregation is enhanced by adding water (left) from the region where the segregation decreases or stays the same (right). From [117].

dissipation tends to enlarge the energy difference between large and small grains, resulting in an enhanced segregation. As liquid content is increased, the liquid bridge becomes larger and the kinetic energy becomes insufficient to break the bridges [117]. Then, segregation is suppressed and the system goes from the intermittent regime to the viscoplastic regime.

3.2.2. Shear experiments for various liquid content. Recently, Fournier *et al.* [27] investigated the response of wet granular materials under shear by using a unique experimental set-up, shown in figure 21. A cylindrical cell was filled with spherical glass beads wet by water, where the flat sides of the cell (area A) each consist of a thin latex membrane. Adjacent to each membrane was a cylindrical chamber filled with liquid, connected to a syringe. When the pistons of the syringe are moved at equal speed, the membranes are deformed by a volume ΔV (figure 21(a) shows a lateral cut of the cylindrical cell (top) and a vertical cut (bottom)), which allows them to shear the granular material under a constant volume at a controlled speed. The pressure at each membrane is measured during the shear. The pressure difference $\Delta\sigma$ between the two membranes versus average shear $\Delta V/A$ is shown in figure 21(b) for densely packed glass beads (packing fraction $\nu \approx 0.63$), showing hysteresis. The vertical width of the hysteresis loop reflects the resistance to shear of the material. They defined $\Delta\sigma_0$ as the vertical width of the hysteresis loop at zero strain divided by two, and measured $\Delta\sigma_0$ for various liquid content and shear rate. The dependence of

$\Delta\sigma_0$ upon the amount of wetting liquid is shown in figure 22. Following their parametrization, the horizontal axis shows W , the ratio of the liquid volume to the total volume. For a given packing fraction ν , the liquid saturation S is given by $S = W/(1 - \nu)$, thus $W = 0.35$ is almost in a saturated state ($S \approx 0.95$) when $\nu = 0.63$. We can see that $\Delta\sigma_0$ increases rapidly as W is increased from zero, but it starts to drop at $W \approx 0.04$ ($S \approx 0.1$) and goes to zero at $W \approx 0.35$. They observed

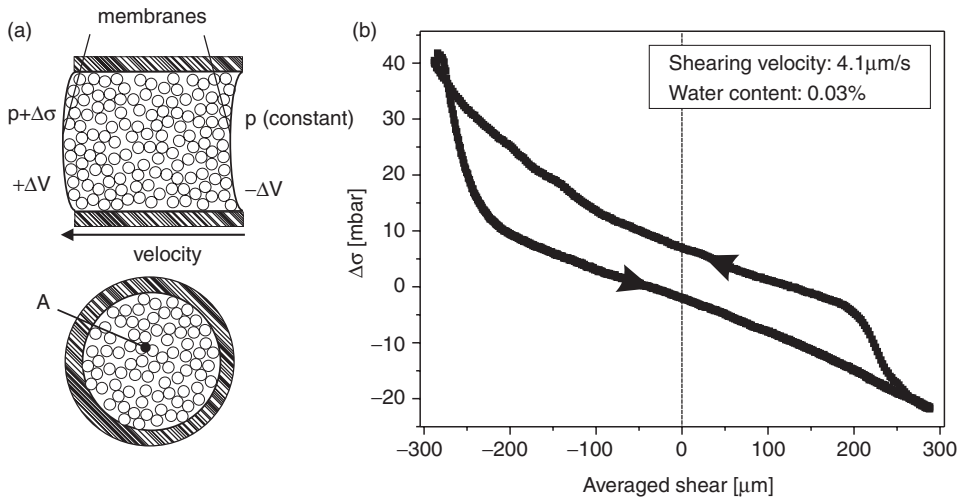


Figure 21. (a) Experimental setup to shear wet granular materials in a cell, showing a slice of the shearing cell seen from the side and from the front. (b) The hysteresis loop of the pressure difference $\Delta\sigma$ versus the average shear $\Delta V/A$ for densely packed glass beads. From [27].

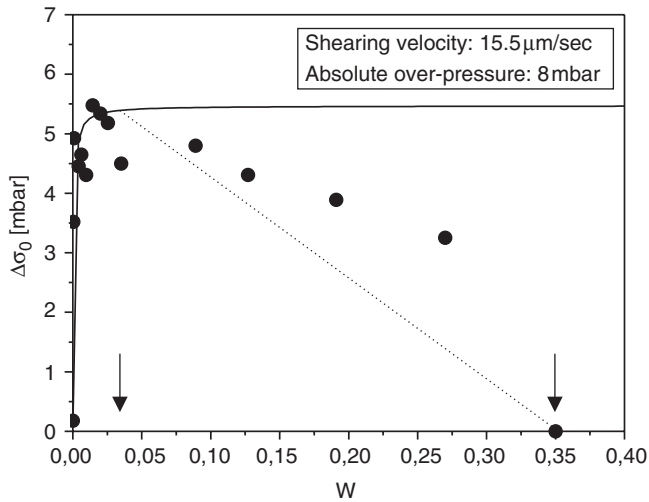


Figure 22. Dependence of $\Delta\sigma_0$ upon the amount of the liquid W . From [27].

the liquid distribution for small liquid content by index matching techniques, and found that $W \approx 0.03$ is the point where liquid bridges start to merge to form a liquid cluster (figure 23); beyond that point, the interfaces between the air and liquid start to decrease, which may cause the decrease of the cohesive force.

Reference [27] also investigated the shear rate dependence of $\Delta\sigma_0$. Within the investigated range of the shear rate, $\Delta\sigma_0$ decreases for larger shear rate, while the dry granular material does not show shear-rate dependence. A possible origin of the shear-rate dependence is the time dependence of liquid motion as described in section 3.2.1, which affect the temporal evolution of liquid bridges.

In addition, they [27] claim that the increase of the shear stress is not solely coming from the frictional effect, as in the Mohr–Coulomb picture described in section 3.1.2, but it can be understood by just considering the cohesion that arises from the liquid bridges. One of the tests they conducted to confirm their claim is to measure the absolute pressure dependence of $\Delta\sigma_0$. The frictional shear stress proportional to the cohesive normal stress σ_c is responsible for the fact that $\Delta\sigma_0$ is greater than that of the dry granular material, then applying a unidirectional pressure comparable with σ_c for *dry* granular material may cause a similar effect to increase $\Delta\sigma_0$. However, they found that applying absolute pressure to the sample is not enough to make $\Delta\sigma_0$ increase. Though the fact that the applied pressure is unidirectional while the cohesive pressure is uniform may be one of the causes of this difference [22], their results indicates that the origin of the higher yield shear stress in wet granular materials need to be investigated further.

The response of materials against shear is a fundamental property to understand the material’s rheology. Further experiments of sheared wet granular material in various set-ups would be useful.

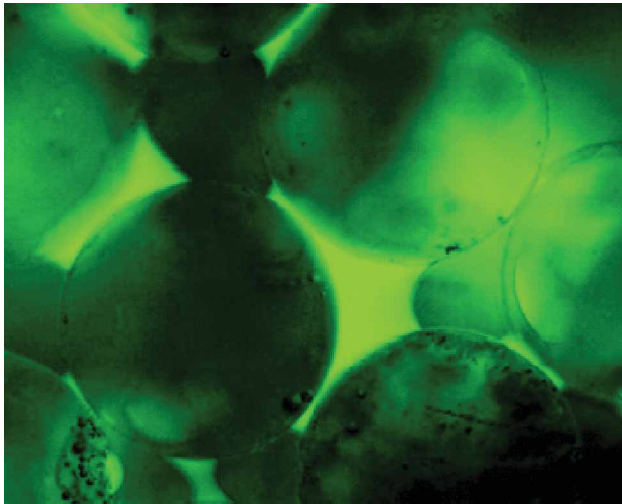


Figure 23. Fluorescence microscope images of liquid distribution between glass beads of diameter $375\ \mu\text{m}$ for $W=0.03$, “liquid clusters” are formed. From [27].

3.2.3. Dynamics of wet granular media: practical applications. There are many research fields that investigate the dynamics of wet granular media from a practical point of view. Below we summarize a few examples.

3.2.3.1. Agglomeration processing: grains bound by liquid. During an agglomeration or granulation process, particles lump or agglomerate together into larger, semi-permanent aggregates called granules [24, 118, 131]. There are several methods to make granules. One of them is to spray a binder liquid onto dry powder and mix them in, e.g. a tumbling drum so that clumps of particles bound by liquid grows. The granules may either grow or break down when they collide. Another method is to strongly shear a very dense mixture of binder liquid and powder (dense paste), and then air comes into the paste to form lumps. In either method, the main source of the cohesive force that binds powder particles together is the capillary force.

Numerous dynamical experiments have been performed on granulation processing; the dynamics of liquid distribution during granulation, the growth of granules, the shear rate dependence of the growth rate, the collision velocity dependence of breakage, and so on. Though most of the experimental set-ups seem rather complicated, the accumulated knowledge provides many insights on the dynamical properties of wet granular media. However, it is beyond the scope of this brief review to summarize all experiments in this subfield. Interested readers should consult a rather recent review on this topic [24], a conference proceedings [118], and references therein.

In addition, the properties of sheared dense paste are important not only in the granulation process, but also in, e.g. ceramics engineering, where the rheology of paste has been investigated. The importance of cohesion due to the capillary effect in the rheology of paste has often been pointed out (e.g. [119, 120]), and the knowledge about its rheology also provides insights about wet granular media.

3.2.3.2. Geological events. Geology is one of the largest research fields on wet granular media. The failure criterion of soils and also their dynamical behaviour are very important to understand. Significant, and sometimes catastrophic and tragic, examples include land slides, debris flows, and liquefaction of ground (see, e.g. [71, 121–124]).

Most of the past work on debris flows focused on the flow of soils saturated by water. In studies of debris flows, knowledge about dry granular media has been incorporated into the analysis, and at the same time, the significant effects of the liquid lubrication and the liquid viscosity on debris flows have been investigated [121]. Liquefaction of wet soils triggered by earthquakes is also often studied in saturated situations [71]. Systematic studies of wet granular media from partially wet to the completely wet state should also provide useful insights to understand these important geological events.

4. Summary and open questions

4.1. Effect of the liquid content on quasi-static behaviour

The cohesive force due to the presence of a liquid arises in the pendular, funicular, and capillary states. This cohesion gives rise to a finite cohesive stress in

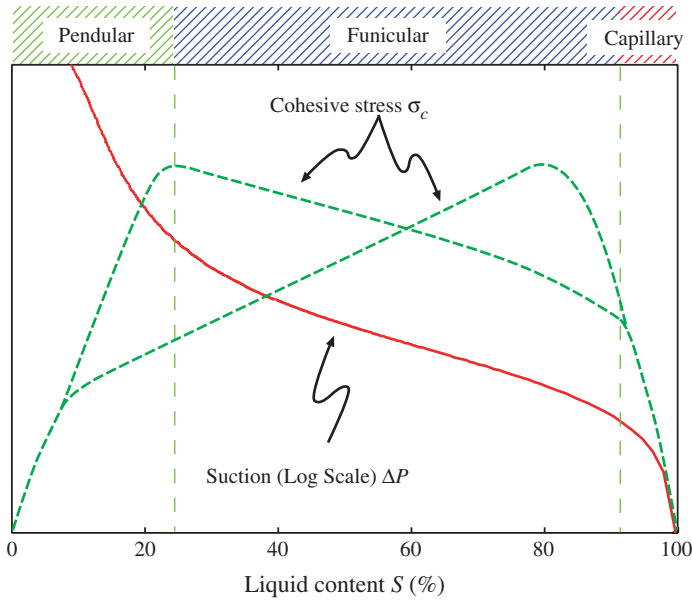


Figure 24. (colour online). Schematic diagram summarizing the variations of the suction ΔP and the cohesive stress σ_c , upon changing the liquid content S .

quasi-static experiments. Figure 24 shows a schematic diagram summarizing how the suction ΔP and the cohesive stress σ_c vary upon liquid content.

The dependence of the suction ΔP on the liquid content S is given by a red solid line, and its slope changes significantly near the phase boundaries between the pendular, funicular, and capillary states, as discussed in subsection 2.2.1.

The cohesive stress σ_c versus S is schematically shown by the green dashed lines. The overlapping dashed curves for low and high S are better established, while the non-overlapping intermediate curves vary significantly between experiments. The cohesive stress σ_c increases as we add more and more liquid to initially dry grains, shown by the positive slope, for small S , of the σ_c line in the pendular state. At the opposite end, cohesion becomes zero for completely saturated granular media ($S = 100\%$), schematically shown by the green dashed line with negative slope for S close to 100% in the capillary state.

In the funicular state, the cohesive stress σ_c dependence on the liquid content S is not clearly understood. The cohesive stress σ_c may either increase or decrease with S in the funicular state. These possible curves are shown by the green dashed lines, where both lines connect to single lines in the limits when $S \rightarrow 0$ and $S \rightarrow 100\%$. We see that there would be at least one maximum of the cohesive stress at a certain liquid content, though it is not clear, *a priori*, the location of the peak.

4.2. Open problems

There are a number of open problems on mechanical properties of wet granular media, some of which have already been mentioned in the text. In this subsection,

we list a few examples of open problems, in order to encourage future studies in this area.

4.2.1. Jamming. As summarized in subsection 4.1, in the quasi-static regime, the cohesion in wet granular media has a maximum for a certain liquid content, though whether the maximum is located at a rather small or large liquid content is not known *a priori*. This variable cohesion will affect the ‘jamming’ properties of the granular assembly. Thus, an interesting problem worth considering is the jamming phase diagram in wet granular media.

A jammed state occurs when a disordered system subject to an external force is caught in a small region of phase space, with no possibility of escape [104, 108, 125–130]. In order to unjam a jammed material, a finite yield stress or fluctuation energy is needed, which forces the elements to escape from the phase space region where they are trapped. Granular media at rest is a typical jammed material, where we need a finite yield stress or external energy input in order to let the grains flow or move. There are many kinds of materials that show jamming, such as dense colloids, and pinned vortices in superconductors. Jamming also plays a role in the mechanical properties of wet granular media. For example, Cates *et al.* [131] recently tried to understand the physics of granulation (section 3.2.3) in a highly sheared dense paste in terms of a jamming transition under shear.

Liu *et al.* [125] proposed a very schematic phase diagram for jamming, in the space of packing fraction ν (density), external load, and temperature or fluctuation energy. The purpose of this schematic phase diagram is to try to summarize a unified view of the jamming phenomena, observed in various media. A schematic diagram of our jamming phase diagram is shown in figure 25; the solid black curves, labelled with the number 0, were proposed by [127, 128] for non-cohesive (dry) granular media. The axes shown are: inverse packing fraction $1/\nu$, the yield stress σ_{yield} , and the fluctuating energy T from an external energy source, such as vibration. One of the features of jamming in dry granular media is that the behaviour in the $T=0$ plane, i.e. no external energy, can be easily investigated. The ‘jammed’ phase-boundary intersects the inverse packing fraction $1/\nu$ axis at zero yield stress and temperature, and the packing fraction at the intersection corresponds to the random closed-packing density [127, 128].

Obviously, attractive interactions modify the jamming properties. Trappe *et al.* [129] investigated jamming in colloidal systems with varying attractive interaction potentials; they found that the jammed phase boundary shifts to higher temperatures for stronger attractive potentials, because the attractive potential characterizes the energy that particles need to escape from the phase space where they are trapped. Jamming in cohesive powders was investigated by [130]; the powder particles were large enough so that thermal noise was negligible. It was found that the critical jamming density for zero fluctuation energy and yield stress for cohesive powder is smaller than the critical density in non-cohesive granular media. This is because the cohesion made it possible to form very sparse but stable clusters of powder. Indeed, a percolating cluster appears in their system for relatively low densities.

Considering these results, the cohesion present in wet granular media will decrease the density needed to jam the system. To break a cluster in wet granular media, a large enough external fluctuation energy is needed, and this energy will

increase with cohesion. The yield stress will increase with cohesion as described by the Mohr–Coulomb criterion, where the yield shear stress increases with the cohesive stress σ_c . These considerations imply that, for cohesive granular media, the volume of phase space occupied by the jammed state expands as the cohesion increases.

How is the jammed phase diagram for granular media modified by adding liquid? A schematic phase diagram is shown in figure 25. The number in each curve there shows how the behaviour changes as we increase liquid content. When a small amount of liquid is added, the phase boundaries are slightly shifted so that the jammed phase expands in all three directions of $1/v$, τ , and T (number 1, green dotted lines). As liquid is further added, the cohesion *increases*, and the boundary will shift further. At a certain liquid content, the cohesion will reach a maximum, corresponding to the *largest jammed region* in phase space (number 2, blue dashed lines). As we further increase the liquid content, the cohesion *decreases*, and the phase-space volume of the jammed region decreases (number 3, red dash-dotted line). Namely, as far as cohesion is concerned, there is an optimal liquid content that maximizes the jammed region. This argument does not consider the effects of liquid other than cohesion. For large enough liquid content, the lubrication effect may affect this conclusion, and could drastically shrink the size of the jammed region. The liquid content dependence of the jamming behaviour in wet granular media is an important and interesting phenomenon that has not been systematically investigated and constitutes a fertile new direction of research.

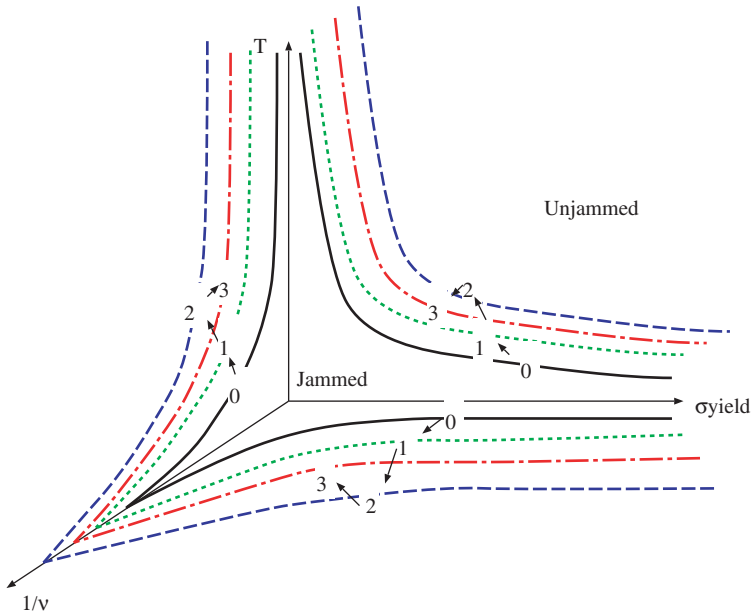


Figure 25. Schematic diagram of a possible jamming phase diagram of granular media for various liquid contents. Number 0 (black solid line): dry . Number 1 (green dotted line): small amount of liquid (slightly cohesive). Number 2 (blue dashed line): ‘optimal’ amount of liquid (the most cohesive, and the largest phase-space volume of the jammed phase). Number 3 (red dash-dotted line): large amount of liquid (less cohesive than the optimal case).

4.2.2. Statistical mechanics approach. Recently, many physicists are trying to describe dry granular systems using statistical mechanics approaches, especially in the jammed regime (For a recent review, see [132]).

Edwards [12, 133] postulated that a dense granular assembly under small external perturbations can take all possible jammed configurations, and the density can be described by suitable ensemble averages over its blocked states. Later, Nowak *et al.* [41] investigated the compaction of slowly tapped granular assemblies, and found there exists a ‘reversible regime’. When a loosely packed configuration is tapped, large voids are removed, which results in irreversible motion of grains (the initial loosely packed configuration cannot be reproduced by further tapping). Once the memory of this initial configuration is lost, after large enough tapping, the density is determined by the ratio Γ of the tapping amplitude to gravity, which is in the reversible regime; in this regime, the density is lower for larger Γ . The existence of a reversible regime is non-trivial in granular matter, where the frictional force depends on history. The Edwards’ scenario only considers non-history dependent situations, and the existence of such a regime gives hope that this scenario would work in the reversible regime. Research to test this theory has been done [134–140], and there remains many open questions.

Another example of a statistical mechanics approach is the recent experiment by [104], who observed the motion of a torsion oscillator immersed in a granular medium perturbed by external vertical tapping, and measured the susceptibility and the auto-correlation function of the motion of the oscillator. For the equilibrium systems, these two quantities are related by the fluctuation-dissipation theorem and the temperature can be consistently determined. They [104] examined whether the same formalism works in the granular state, and found that an ‘effective temperature’ can be defined from the susceptibility and the auto-correlation function. Though this dissipative system is far from equilibrium, the analogy to the fluctuation-dissipation theorem in the experiment is remarkable. It is an interesting question whether such a relation can be extended to other systems or regimes (e.g. wet grains).

In the case of wet granular media, the available phase space is larger and, due to the cohesion, the history dependence is stronger than the dry case as mentioned in Section 3.1.1 and Table 1. Future experiments probing the statistical mechanics in wet granular assemblies will provide more knowledge of its applicability and generality.

4.2.3. Arches and contact-force fluctuations. Arches (i.e. effective long-range interactions) and the resulting large fluctuation of contact forces have been extensively studied in several types of dry granular media (see, e.g. [141–147]). However, no such systematic studies exist for wet granular media. The clogging of cohesive powders in a hopper is often said to be an arching effect [3], but it is rather rare to investigate the arches directly in partially wet granular media. This would be interesting because the change of the inter-particle forces with liquid content likely affects the strength and topology of the so-called ‘force chains’ or stress-line-networks of the granular assembly.

4.2.4. Simple experimental set-ups to study the dynamics of wet granular media. Several experimental set-ups have been widely performed to study the fundamental dynamics of dry granular media. The widely used set-ups include vibrated granular media (e.g. [96, 102–108]), rotating drums (e.g. [85–92]), shear

(e.g. [145, 148–150]), and inclined chutes (e.g. [13, 151–159]). These set-ups have played important roles in studying the fundamental dynamics and rheology of dry granular materials.

Some of the set-ups have been used in recent experiments of wet granular media, as discussed in section 3.2, but not many systematic studies have been done so far. One of the difficulties in fundamental studies of wet granular materials is their strong tendency to be inhomogeneous. It becomes difficult to induce particle motions, due to cohesive force. In other words, the regions that were mobile in the dry case become localized when wet, and the bulk material becomes solid. Similar behaviour is known for dry granular materials as well (e.g. shear bands), but the localization would be stronger for the wet case. In addition, the distribution of liquid can also be inhomogeneous, especially for larger liquid content. Nonetheless, further studies on the dynamics of wet granular materials (including their inhomogeneity) using these rather simple set-ups will certainly contribute to granular science.

4.2.5. Numerical simulations. The recent remarkable progress in the study of dry granular material is partially due to numerical simulations. Molecular dynamics simulations of soft-sphere or inelastic hard-sphere models help clarify phenomena found in experiments and get data in ‘ideal’ situations. In the case of wet granular media, however, its numerical simulation model for the wide range of liquid content has not been established yet because of its complexity.

Some models of wet grains in the pendular state have been proposed for molecular dynamics simulations (e.g. [24, 51, 118, 160–163]), where most of them are based on soft-particle models for dry granular materials with elastic force and dissipation [164]. In models for wet grains, the effect of the liquid is added by assuming that liquid bridges are formed when grains are in contact, and cohesion and dissipation due to the liquid bridges are taken into account. These types of models would be applicable to some extent to situations where the amount of liquid is small and the liquid mostly sticks to the grain surface. However, as the liquid content is increased, the liquid-bridge picture becomes invalid and liquid motion becomes relevant. No available simple models has been yet proposed for this regime, as far as we know.

Even for dry granular media, the real granular particles are more complicated than the ones used in most computational models; still, the simple models have been found to be very useful. It is apparent that good models are also needed for wet granular material. The required level of realism of the model largely depends on the phenomena that one would like to understand. To help the modeling, more systematic experiments in simple situations are necessary.

4.2.6. Mechanical properties of snow. The mechanical properties of snow have been investigated for a long time (e.g. [54, 165–169]). It is important to understand snow properties to reduce disasters caused by snow avalanches; thus knowledge should also be useful to design equipment and constructions in snowbound areas [169].

Snow is a type of granular material of grains of ice. Snow partially melts in many situations, and pores are filled with both air and water; it is a ‘wet granular material’. The knowledge obtained about the dynamics of dry granular media has been found to be useful to understand snow dynamics; for example, the mechanism of size

segregation is important to understand how to save skiers caught in an avalanche [167]. In terms of cohesion among grains, wet snow avalanches has some aspects in common with avalanches in partially wet granular media [84]. More research on wet granular media should be useful to better understand the mechanical properties of snow.

However, there is a big difference between wet sands and snow; in snow, solid ice-bonds exist between ice grains. In new or low-density snows, ice grains slide over each other, while in old or dense snow, the deformation of solid ice-bonds dominate the interactions [167]. The formation, strength, and breakage of ice-bonds depend on many factors such as the heat flux and motion of water or water vapours. Because of this complex nature of interactions, there remains many open questions in snow physics. For example, it is known that the density of snow is not a good parameter to characterize snow properties, and one needs to classify snow by considering its microstructure [169]. It will be useful to find a parameter that is easily measured and can better characterize its mechanical properties.

5. Conclusion

Wet granular media have properties which are significantly different from dry grains. These include enhanced cohesion among grains leading to very steep angles of repose. Wet granular media are pervasive everywhere, including numerous industrial applications and geological phenomena. In spite of the ubiquitous presence of wet granular media and its importance, relatively little is known about it. This brief overview sketched some of the physical properties of wet granular media, and identified several open problems for future studies.

Acknowledgements

NM thanks H. Nakanishi for helpful discussions. The authors thank G. D'Anna for his comments on an early version of the manuscript. Part of this work has been done when NM was supported by the Special Postdoctoral Researcher Program by RIKEN. NM is supported in part by a Grant-in-Aid for Young Scientists(B) 17740262 from The Ministry of Education, Culture, Sports, Science and Technology (MEXT) and Grant-in-Aid for Scientific Research (C) 16540344 from the Japan Society for the Promotion of Science (JSPS). FN is supported in part by the National Security Agency (NSA) and Advanced Research and Development Activity (ARDA) under Air Force Office of Research (AFOSR) contract number F49620-02-1-0334, and by the National Science Foundation grant No. EIA-0130383.

References

- [1] J. Duran, *Sands, Powders, and Grains: An Introduction to the Physics of Granular Materials* (Springer, New York, 1997).
- [2] H.M. Jaeger, S.R. Nagel and R.P. Behringer, *Rev. Mod. Phys.* **68** 1259 (1996).
- [3] R.M. Nedderman, *Statics and Kinematics of Granular Matter* (Cambridge University Press, Cambridge, 1992).

- [4] P.-G. de Gennes, *Rev. Mod. Phys.* **71** S374 (1999).
- [5] R.P. Behringer and J.T. Jenkins (Editors), *Powders & Grains 97* (A.A. Balkema, Rotterdam, 1997).
- [6] R.A. Bagnold, *The Physics of Blown Sand and Desert Dunes*, (Mathuen, London, 1941).
- [7] H.M. Jaeger and S.R. Nagel, *Science* **255** 1523 (1992).
- [8] H.M. Jaeger, S.R. Nagel and R.P. Behringer, *Physics Today* **49** 32 (1996).
- [9] P. Sholtz, M. Bretz and F. Nori, *Contemporary Physics* **38** 329 (1997).
- [10] F. Nori, P. Sholtz and M. Bretz, *Scientific American* **277** 84 (1997).
- [11] R.P. Behringer, H.M. Jaeger and S.R. Nagel (Editors), *Chaos* **9** 509 (1999).
- [12] S.F. Edwards and D.V. Grinev, *Adv. Phys.* **51** 1669 (2002).
- [13] M. Bretz, J.B. Cunningham, P.L. Kurczynski and F. Nori, *Phys. Rev. Lett.* **69** 2431 (1992).
- [14] Kansai International Airport Co. Ltd. *Brief Summary of Settlement*, <http://www.kiac.co.jp/english/land/land.htm>.
- [15] Y. Kimura and H. Okabe, *Tribology Gairon* (in Japanese) (Yokendo, Tokyo, 1994).
- [16] O. Pinkus and B. Sternlicht, *Theory of Hydrodynamic Lubrication* (McGraw-Hill, New York, 1961).
- [17] F.P. Bowden and D. Tabor, *The Friction and Lubrication of Solids* (Clarendon Press, Oxford, 1986).
- [18] J.-C. Géminard, W. Losert and J.P. Gollub, *Phys. Rev. E* **59** 5881 (1999).
- [19] M. Medved, H.M. Jaeger and S.R. Nagel, *Phys. Rev. E* **63** 061302 (2001).
- [20] L.D. Landau and E.M. Lifshitz, *Fluid Mechanics*, 2nd edn (Butterworth-Heinemann, Oxford, 1987).
- [21] C.D. Willett, M.J. Adams, S.A. Johnson and J.P.K. Seville, *Langmuir* **16** 9396 (2000).
- [22] S. Herminghaus, *Adv. Phys.* **54** 221 (2005).
- [23] D.M. Newitt and J.M. Conway-Jones, *Trans. I. Chem. Eng.* **36** 422 (1958).
- [24] S.M. Iveson, J.D. Litster, K. Hapgood and B.J. Ennis, *Powder Technol.* **117** 3 (2001).
- [25] M.A. Rubio, C.A. Edwards, A. Dougherty and J.P. Gollub, *Phys. Rev. Lett.* **63** 1685 (1989).
- [26] T.G. Mason, A.J. Levine, D. Ertas and T.C. Halsey, *Phys. Rev. E* **60** R5044 (1999).
- [27] Z. Fournier, D. Geromichalos, S. Heminghaus, M.M. Kohonen, F. Mugele, M. Scheel, M. Schulz, B. Schulz, Ch. Schier, R. Seemann and A. Skudelný, *J. Phys.: Condens. Matter* **17** S477 (2005).
- [28] N. Lu and W.J. Likos, *Unsaturated Soil Mechanics* (John Wiley, Hoboken, 2004).
- [29] D.K. Cassel and A. Klute, in *Methods of Soil Analysis, Part 1, Physical and Mineralogical Methods*, 2nd edn, edited by A. Klute (Soil Science Society of America, Madison, WI, 1986).
- [30] D.I. Stannard, *Geotech. Test. J.* **15** 48 (1992).
- [31] J.W. Hilf, An investigation of pore water pressure in compacted cohesive soils Technical report, United States Department of the Interior, Bureau of Reclamation, Design and Construction Division, Denver, CO, 1956.
- [32] K.A. Bocking and D.G. Fredlund, In *Proceedings of the 4th International Conference on Expansive Soils* (Denver, CO, 1980), pp. 117–135.
- [33] C.J. Phene, G.J. Hoffman and S.L. Lawlings, *Soil Science Society of America Proceedings* **35** 27 (1971).
- [34] C.J. Phene, G.J. Hoffman and S.L. Lawlings, *Soil Science Society of America Proceedings* **35** 225 (1971).
- [35] D.G. Fredlund and D.K.H. Wong, *Geotech. Test. J.* **12** 188 (1989).
- [36] S.L. Houston, W.N. Houston and A. Wagner, *Geotech. Test. J.* **17** 185 (1994).
- [37] P.-G. de Gennes, *Rev. Mod. Phys.* **57** 827 (1985).
- [38] P.-G. de Gennes, D. Quere and F. Brochard-Wyart, *Capillarity and Wetting Phenomena: Drops, Bubbles, Pearls, Waves* (Springer-Verlag, Berlin, 2003).
- [39] M. Alava, M. Dubé and M. Rost, *Adv. Phys.* **53** 83 (2004).
- [40] J.B. Knight, C.G. Fandrich, C.N. Lau, H.M. Jaeger and S.R. Nagel, *Phys. Rev. E* **51** 3957 (1995).

- [41] E.R. Nowak, J.B. Knight, E. Ben-Naim, H.M. Jaeger and S.R. Nagel, *Phys. Rev. E* **57** 1971 (1998).
- [42] M. Nicodemi, A. Coniglio and H.J. Herrmann, *Phys. Rev. E* **55** 3962 (1997).
- [43] J.Q. Xu, R.P. Zou and A.B. Yu, *Phys. Rev. E* **69** 032301 (2004).
- [44] G. Gioia, A.M. Cuitiño, S. Zheng and T. Uribe, *Phys. Rev. Lett.* **88** 204302 (2002).
- [45] C.M. Kong and J.J. Lannutti, *J. Am. Ceram. Soc.* **83** 685 (2000).
- [46] L. Bocquet, E. Charlaix, S. Ciliberto and J. Crassous, *Nature* **396** 735 (1998).
- [47] D.J. Hornbaker, R. Albert, I. Albert, A.-L. Barabási and P. Schiffer, *Nature* **387** 765 (1997).
- [48] R. Albert, I. Albert, D. Hornbaker, P. Schiffer and A.-L. Barabási, *Phys. Rev. E* **56** R6271 (1997).
- [49] N. Fraysse, H. Thomé and L. Petit, *Euro. Phys. J. B* **11** 615 (1999).
- [50] T.C. Halsey and A.J. Levine, *Phys. Rev. Lett.* **80** 3141 (1998).
- [51] S.T. Nase, W.L. Vargas, A.A. Abatan and J.J. McCarthy, *Powder Technol.* **116** 214 (2001).
- [52] F. Restagno, C. Ursini, H. Gayvallet and E. Charlaix, *Phys. Rev. E* **66** 021304 (2002).
- [53] G. Ovarlez, E. Kolb and E. Clement, *Phys. Rev. E* **64** 060302 (2001).
- [54] G. D'Anna, *Phys. Rev. E* **62** 982 (2000).
- [55] G. D'Anna, *Europhys. Lett.* **51** 293 (2000).
- [56] A.J. Forsyth, S. Hutton and M.J. Rhodes, *Powder Technol.* **126** 150 (2004).
- [57] J. Crassous, L. Bocquet, S. Ciliberto and C. Laroche, *Europhys. Lett.* **47** 562 (1999).
- [58] J.N. Israelachvili, *Intermolecular and Surface Forces*, 2nd edn (Academic Press, New York, 1992).
- [59] N. Olivi-Tran, N. Fraysse, P. Girard, M. Ramonda and D. Chatain, *Eur. Phys. J. B* **25** 217 (2002).
- [60] H. Rumpf, in *Agglomeration*, edited by W. A. Knepper (Interscience, New York, 1962), pp. 379.
- [61] J.W. Cahn and R.B. Heady, *J. Am. Ceram. Soc.* **53** 406 (1970).
- [62] M.M. Kohonen, D. Geromichalos, M. Scheel, C. Schier and S. Herminghaus, *Physica A* **339** 7 (2004).
- [63] P. Tegzes, R. Albert, M. Paskvan, A.-L. Barabási, T. Vicsek and P. Schiffer, *Phys. Rev. E* **60** 5823 (1999).
- [64] D. Ertas, T.C. Halsey, A.J. Levine and T.G. Mason, *Phys. Rev. E* **66** 051307 (2002).
- [65] S. Nowak, A. Samadani and A. Kudrolli, *Nature Physics* **1** 50 (2005).
- [66] D.G. Bika, M. Gentzler and J.N. Michaels, *Powder Technol.* **117** 98 (2001).
- [67] H. Schubert, *Powder Technol.* **11** 107 (1975).
- [68] A.T. Procopio, A. Zavaliangos, J.C. Cunningham, *J. Materials Sci.* **38** 3629 (2003).
- [69] H. Hertz, *Gesammelte Werke* (Collected Works) (Leipzig, 1895).
- [70] Á. Kézdi, *Soil Physics: Handbook of Soil Mechanics*, Vol. 1 (Elsevier, Amsterdam, 1974).
- [71] F. Oka, *Soil Mechanics* (Doshitsu-Rikigaku, in Japanese) (Asakura-Shoten, Tokyo, 2003).
- [72] P. Pierrat, D.K. Agrawal and H.S. Caram, *Powder Technol.* **99** 220 (1998).
- [73] P. Pierrat and H.S. Caram, *Powder Technol.* **91** 83 (1997).
- [74] H. Schubert, W. Herrmann and H. Rumpf, *Powder Technol.* **11** 121 (1975).
- [75] H.G. Kristensen P. Holm, T. Schaefer, *Powder Technol.* **43** 213 (1985).
- [76] H.C. Kristensen, E. Holii and T. Schaefer, *Powder Technol.* **44** 227 (1985).
- [77] V. Escario, in *Proceedings of the 4th International Conference on Expansive Soils* (Denver, CO, 1980), pp. 781–787.
- [78] V. Escario, J. Juca and M.S. Coppe, in *Proceedings of the 12th International Conference on Soil Mechanics and Foundation Engineering*, **3** (Rio de Janeiro, 1989), pp. 43–46.
- [79] A.W. Bishop, I. Alpan, G.E. Blight and I.B. Donald, in *ASCE Research Conference on the Shear Strength of Cohesive Soils* (University of Colorado, Boulder, 1960), pp. 503–532.
- [80] D.Y.F. Ho and D.G. Fredlund, in *Proceedings of the ASCE Geotechnical Conference Engineering and Construction in Tropical and Residual Soils* (Honolulu, HI, 1982).
- [81] J. Krahn, D.G. Fredlund and M.J. Klassen, *Can. Geotech. J.* **26** 269 (1989).
- [82] J.K.M. Gan, D.G. Fredlund and H. Rahardjo, *Can. Geotech. J.* **25** 500 (1988).

- [83] S.K. Vanapalli, D.G. Fredlund, D.E. Pufahl and A.W. Clifton, *Can. Geotech. J.* **33** 379 (1996).
- [84] P. Tegzes, T. Vicsek and P. Schiffer, *Phys. Rev. E* **67** 051303 (2003).
- [85] J. Rajchenbach, *Phys. Rev. Lett.* **65** 2221 (1990).
- [86] J. Rajchenbach, *Phys. Rev. Lett.* **88** 014301 (2002).
- [87] D. Bonamy, F. Daviaud, L. Laurent M. Bonetti and J.P. Bouchaud, *Phys. Rev. Lett.* **89** 034301 (2002).
- [88] J. Rajchenbach, *Adv. Phys.* **49** 229 (2000).
- [89] V.G. Benza, F. Nori and O. Pla, *Phys. Rev. E* **48** 4095 (1993).
- [90] G.H. Ristow, *Europhys. Lett.* **34** 263 (1996).
- [91] D.V. Khakhar, J.J. McCarthy, T. Shinbrot and J.M. Ottino, *Phys. Fluids* **9** 31 (1997).
- [92] G. Baumann, J.M. Janosi and D.E. Wolf, *Phys. Rev. E* **51** 1879 (1995).
- [93] A. Castellanos, J.M. Valverde, A.T. Perez, A. Ramos and P.K. Watson, *Phys. Rev. Lett.* **82** 1156 (1999).
- [94] P. Tegzes, T. Vicsek and P. Schiffer, *Phys. Rev. Lett.* **89** 094301 (2002).
- [95] T. Poschel and S. Luding (Editors), *Granular Gases*, volume 564 of *Lecture Notes in Physics*. (Springer-Verlag, Berlin, 2001).
- [96] A. Kudrolli, *Rep. Prog. Phys.* **67** 209 (2004).
- [97] G.H. Ristow, *Pattern Formation in Granular Materials* (Springer-Verlag, Berlin, 2000).
- [98] E. Clément, J. Duran and J. Rajchenbach, *Phys. Rev. Lett.* **69** 1189 (1992).
- [99] J. B. Knight, H. M. Jaeger and S. R. Nagel, *Phys. Rev. Lett.* **70** 3782 (1993).
- [100] S. Renard, T. Schwager, T. Pöschel and C. Saluena, *Eur. Phys. J. E* **4** 233 (2001).
- [101] T. Pöschel, T. Schwager and C. Saluena, *Phys. Rev. E* **62** 1361 (2000).
- [102] W. Losert, D.G.W. Cooper and J.P. Gollub, *Phys. Rev. E* **59** 5855 (1999).
- [103] F. Melo, P.B. Umbanhowar and H.L. Swinney, *Phys. Rev. Lett.* **75** 3838 (1995).
- [104] G. D'Anna, P. Mayor, A. Barrat, V. Loreto and F. Nori, *Nature* **424** 909 (2003).
- [105] P.B. Umbanhowar, F. Melo and H.L. Swinney, *Nature* **382** 793 (1996).
- [106] H.K. Pak and R.P. Behringer, *Nature* **371** 231 (1994).
- [107] C. Laroche, S. Douady and S. Fauve, *J. Physique* **50** 699 (1989).
- [108] G. D'Anna and G. Gremaud, *Phys. Rev. E* **64** 011306 (2001).
- [109] M. Schell, D. Geromichalos and S. Herminghaus, *J. Phys.: Condens. Matter* **16** S4213 (2004).
- [110] M.E. Mobius, B.E. Lauderdale, S.R. Nagel and H.M. Jaeger, *Nature* **414** 270 (2001).
- [111] D.C. Hong, P.V. Quinn and S. Luding, *Phys. Rev. Lett.* **86** 3423 (2001).
- [112] J.M. Ottino and D.V. Khakhar, *Annu. Rev. Fluid Mech.* **32** 55 (2000).
- [113] A. Samadani and A. Kudrolli, *Phys. Rev. Lett.* **85** 5102 (2000).
- [114] A. Samadani and A. Kudrolli, *Phys. Rev. E* **64** 051301 (2001).
- [115] O. Pitois, P. Moucheront and X. Chateau, *J. Colloid Interface Sci.* **231** 26 (2000).
- [116] O. Pitois, P. Moucheront and X. Chateau, *Euro. phys. J. B* **23** 79 (2001).
- [117] D. Geromichalos, M.M. Kohonen, F. Mugele and S. Herminghaus, *Phys. Rev. Lett.* **90** 168702 (2003).
- [118] A.D. Salman and M.J. Hounslow (Editors), *Special Issue: 1st International Workshop on Granulation*, *Powder Technol.* **140** 155–296 (2004).
- [119] J.S. Reed, *Principles of Ceramics Processing*, 2nd edn (John Wiley, New York, 1995).
- [120] H. Van Damme, S. Mansoutre, P. Colombet, C. Lesaffre and D. Picart, *C. R. Physique* **3** 229 (2002).
- [121] R.M. Iverson, *Rev. Geophys.* **35** 245 (1997).
- [122] R. Dikau, D. Brunnsden, L. Schrott and M.-L. Ibsen, *Landslide Recognition* (Wiley, Chichester, 1996).
- [123] P. Coussot, *Mudflow Rheology and Dynamics* (Balkema, Rotterdam, 1997).
- [124] K. Ishihara, *Geotechnique* **43** 351 (1993).
- [125] A.J. Liu and S.R. Nagel, *Nature* **396** 21 (1998).
- [126] A.J. Liu and S.R. Nagel (Editors), *Jamming and Rheology: Constrained Dynamics on Microscopic and Macroscopic Scales* (Taylor & Francis, London, 2001).
- [127] C.S. O'Hern, S.A. Langer, A.J. Liu and S.R. Nagel, *Phys. Rev. Lett.* **88** 075507 (2002).
- [128] C.S. O'Hern, L.E. Silbert, A.J. Liu and S.R. Nagel, *Phys. Rev. E* **68** 011306 (2003).

- [129] V. Trappe, V. Prasad, L. Cipelletti, P.N. Segre and D.A. Weitz, *Nature* **411** 772 (2001).
- [130] J.M. Valverde, M.A.S. Quintanilla and A. Castellanos, *Phys. Rev. Lett.* **92** 258303 (2004).
- [131] M.E. Cates, M.D. Haw and C.B. Holmes, *J. Phys.: Condens. Matter* **17** S2517 (2004).
- [132] P. Richard, M. Nicodemi, R. Delannay, P. Ribi re and D. Bideau, *Nature Materials* **4** 121 (2005).
- [133] S.F. Edwards, in *Granular Matter: An Interdisciplinary Approach* (Springer, New York, 1994), pp. 121–140.
- [134] J.J. Brey, A. Padros and B. Sanchez-Rey, *Physica A* **275** 310 (2000).
- [135] G. Tarjus and P. Viot, *Phys. Rev. E* **69** 011307 (2004).
- [136] M. Nicodemi, *Phys. Rev. E* **82** 3734 (1999).
- [137] A. Coniglio and M. Nicodemi, *Physica A* **296** 451 (2001).
- [138] H.A. Makse and J. Kurchan, *Nature* **415** 614 (2002).
- [139] A. Fierro, M. Nicodemi and A. Coniglio, *Phys. Rev. E* **66** 061301 (2002).
- [140] M. Nicodemi, A. Fierro and A. Coniglio, *Europhys. Lett.* **60** 684 (2002).
- [141] R.R. Hartley and R.P. Behringer, *Nature* **421** 928 (2003).
- [142] I. Albert, P. Tegzes, B. Kahng, R. Albert, J.G. Sample, M. Pfeifer, A.-L. Barab si, T. Vicsek and P. Schiffer, *Phys. Rev. Lett.* **84** 5122 (2000).
- [143] C.-H. Liu, S.R. Nagel, D.A. Schecter, S.N. Coppersmith, S. Majumdar, O. Narayan and T.A. Witten, *Science* **269** 513 (1995).
- [144] D. Howell, R.P. Behringer and C. Veje, *Phys. Rev. Lett.* **82** 5241 (1999).
- [145] B. Miller, C. O'Hern and R.P. Behringer, *Phys. Rev. Lett.* **77** 3110 (1996).
- [146] S.N. Coppersmith, C.-H. Liu, S. Majumdar, O. Narayan and T. A. Witten, *Phys. Rev. E* **53** 4673 (1996).
- [147] D.L. Blair, N.W. Mueggenburg, A.H. Marshall, H.M. Jaeger and S.R. Nagel, *Phys. Rev. E* **63** 041304 (2001).
- [148] H. Xu, M.Y. Louge and A. Reeves, *Continuum Mech. Thermodyn.* **15** 321 (2003).
- [149] D.M. Mueth, G.F. Debregeas, G.S. Karczmar, P.J. Eng, S.R. Nagel and H.M. Jaeger, *Nature* **406** 385 (2000).
- [150] S. Nasuno, A. Kudrolli and J.P. Gollub, *Phys. Rev. Lett.* **79** 949 (1997).
- [151] T. P schel, *J. Physique II* **3** 27 (1993).
- [152] N. Mitarai, H. Hayakawa and H. Nakanishi, *Phys. Rev. Lett.* **88** 174301 (2002).
- [153] N. Mitarai and H. Nakanishi, *Phys. Rev. E* **67** 021301 (2003).
- [154] N. Mitarai and H. Nakanishi, *J. Fluid Mech.* **507** 309 (2004).
- [155] N. Mitarai and H. Nakanishi, *Phys. Rev. Lett.* **94** 128001 (2005).
- [156] O. Pouliquen, *Phys. Fluids* **11** 542 (1999).
- [157] A. Daerr and S. Douady, *Nature* **399** 241 (1999).
- [158] S.B. Savage and K. Hutter, *J. Fluid Mech.* **199** 177 (1989).
- [159] T.S. Komatsu, S. Inagaki, N. Nakagawa and S. Nasuno, *Phys. Rev. Lett.* **86** 1757 (2001).
- [160] T. Gr ger, U. T z n and D.M. Heyes, *Powder Technol.* **133** 203 (2003).
- [161] M. Schulz, B.M. Schulz and S. Herminghaus, *Phys. Rev. E* **67** 052301 (2003).
- [162] G. Lian, C. Thornton and M.J. Adams, *Chem. Eng. Sci.* **58** 3381 (1998).
- [163] M. Hakuno and K. Meguro, *J. Eng. Mech.-ASCE* **119** 1709 (1993).
- [164] P.A. Cundall and O.D.L. Strack, *Geotechnique* **29** 47 (1979).
- [165] M. Fukue, *Mechanical Performance of Snow under Loading* (Tokai University Press, Tokyo, 1979).
- [166] F. Nicor, *Gran. Matt.* **6** 47 (2004).
- [167] P. Bartelt and B. Othmar, *Physics World* **14** 25 (2001).
- [168] G. Seligman, *Snow Structure and Ski Fields* (MacMillan, London, 1936).
- [169] L.H. Shapiro, J.B. Johnson, M. Sturm and G.L. Blaisdell, *Snow mechanics: Review of the state of knowledge and applications* Cold Regions Research and Engineering Laboratory Report, No. 97-3, 1997.